The following publication Y. Tang, W. Liu, K. T. Chau, Y. Hou and J. Guo, "Stochastic Behavior Modeling and Optimal Bidirectional Charging Station Deployment in EV Energy Network," in IEEE Transactions on Intelligent Transportation Systems, vol. 26, no. 5, pp. 6231-6247, May 2025 is available at https://doi.org/10.1109/TITS.2025.3553513.

IEEE TRANSACTIONS ON INTELLIGENT TRANSPORTATION SYSTEMS, VOL. X, NO. X, XXXX

Stochastic Behavior Modelling and Optimal Bidirectional Charging Station Deployment in EV Energy Network

Yao Tang, Student Member, IEEE, Wei Liu, Senior Member, IEEE, Kwok Tong Chau, Fellow, IEEE, Yunhe Hou, Senior Member, IEEE, and Jian Guo, Member, IEEE

Abstract— Electric vehicle energy network (EVEN) enables the transmission of renewable energy from rural to urban area by the flexibility of EVs via energy exchange. In this paper, (dis)charging behavior modelling and bidirectional charging station (BCS) deployment optimization are addressed, since they are crucial in EVEN for EV accommodation, renewable energy utilization, drivers' profitability estimation, operators' cost assessment, and financial policy establishment. A novel stochastic Markov (dis)charging behavior model is proposed to calculate the spatiotemporal load pattern considering the realistic factors such as personal features, state of charge (SoC), electricity price, and BCS locations. Unlike most works ignoring energy trading, six scenarios are explored: (S1) no trade; (S2) trade in main battery. (S3) trade in extra battery. (S4) trade in extra ultracapacitor; (S5) trade in both main and extra battery; (S6) trade in both main battery and ultracapacitor. Also, a multiobjective BCS deployment strategy is newly designed, aiming at minimizing installation cost and driver's electricity bill, while quality of service (QoS) and voltage stability are ensured. An improved hybrid algorithm is developed, which combines hill climbing for enhanced exploitation and particle swarm optimization for better evolvement based on genetic algorithm framework. The simulation validates the fitting ability of charging model, the effectiveness of parameter selection algorithm and the deployment approach. Comparing 6 scenarios, benefits of energy trading in EVEN is confirmed and the superiority of ultracapacitor for trading is demonstrated. The feasibility of financial policies is also studied, and certain guidance is provided for drivers to improve their cost.

Index Terms—Electric vehicle, driver's behavior, bidirectional charging station deployment, energy trading

Nomenclature

Indices and Sets

i, j	Index of nodes in road or in route.
k	Index of routes/EVs.
t	index of time.
l, λ	index of SoC level and price level.

Manuscript received X, X; revised X, X; accepted X, X. This work was supported by two grants (Project No. 17206222 and T23-701/20-R) from the Hong Kong Research Grants Council, Hong Kong Special Administrative

Region, China. (Corresponding author: Kwok Tong Chau.)

Yao Tang, Yunhe Hou and Jian Guo are with Department of Electrical and Electronic Engineering, The University of Hong Kong, Hong Kong, China. (emails: tangyao@eee.hku.hk; yhhou@eee.hku.hk; guojian@eee.hku.hk).

Kwok Tong Chau and Wei Liu is with Research Centre for Electric Vehicles and Department of Electrical and Electronic Engineering, The Hong Kong Polytechnic University, China. (k.t.chau@polyu.edu.hk; wei.liu@polyu.edu.hk).

CS , $CS_{j,k}$	Set of BCSs and BCSs near $r_{j,k}$.
$CS_{j,k}^{access}$	Set of accessible BCSs at at $r_{j,k}$.
V	Set of nodes in road network.
R, R_k	Set of routes, and nodes in k-th route
N^{bus}	Set of buses in the system.

11	Set of cuses in the system.
Parameters	
cost operator	Cost of operator for building BCSs.
$cost^{CS}$, $cost^{server}$	Cost of one BCS and one charging server.
cost driver	Cost of driver's EV bill.
cost ^{elec}	Cost of driver to buy electricity.
cost ^{degrad}	Cost of battery degradation.
$cost_k^b$, $cost_k^{degrad}$	Battery and degradation cost for k-th EV.
c(l), r(l), d(l)	States of charging, running, and discharging.
cap_k	Battery capability of k-th EV.
$cap_k^{\scriptscriptstyle ini}$	Initial battery capability of k-th EV.
$dt_{j,k}^{ m max}$	Maximum allowable distance at $r_{j,k}$.
$dt(r_1,r_2)$	Distance between nodes r_1 and r_2 .
$e_{\scriptscriptstyle k}^{\scriptscriptstyle consume}$	Energy consumed per unit distance.
$e^{remain}_{j,k}$	Remaining energy of destination at $r_{j,k}$.
k_p, k_q	Driver's decisiveness parameter.
m^{\max}	Maximum customer.
n_i , n^{\max}	Number of servers and its maximum value.
$prob_m(t)$	The probabilities that m customers in the
mui o o(4)	system at time t.
price(t) profit ^{trade}	Electricity price at <i>t</i> . Profit of driver via selling electricity.
projii pro ^{pass}	Proportion of fleet that can reach BCSs with
pro	in certain distance.
$p^{ch}(l), q^{ch}(l)$	p and q of main battery for charging.
$p^{dch}(l), q^{dch}(l)$	p and q of main battery for discharging.
	p and q of second device for trading.
$pf^{ch}(t), pf^{dch}(t)$	
$pf_b^{ch}(t), pf_b^{dch}(t)$	
$pf_u^{ch}(t), pf_u^{dch}(t)$	(Dis)charging profile of ultracapacitor.

 $pf_{j,k}^{ch}(t)$, $pf_{j,k}^{dch}(t)$ Charging and discharging demand at $r_{i,k}$.

Non-EV load at node *i*.

 $pf_i^{ch}(t), pf_i^{dch}(t)$ (Dis)charging profile at node i.

© 2025 IEEE. Personal use of this material is permitted. Permission from IEEE must be obtained for all other uses, in any current or future media, including reprinting/republishing this material for advertising or promotional purposes, creating new collective works, for resale or redistribution to servers or lists, or reuse of any copyrighted component of this work in other works.

P_i^{gen}, P_i^{bus}	Active generated power and load at node <i>i</i> .
Q_i^{gen}, Q_i^{bus}	Reactive generated power and load at node <i>i</i> .
r_i	<i>i</i> -th node on the road network.
$r_{j,k}$	<i>j</i> -th node of <i>k</i> -th route.
rt_b , rt_u	(Dis)charging rate of battery and
	ultracapacitor.
rt_k^{ch} , rt_k^{dch}	Charging and discharging rate of <i>k</i> -th EV.
$soc_{j,k}$	EV's SoC at $r_{j,k}$.
$SOC_{j,k}^{remain}$	Remaining SoC of destination at $r_{j,k}$.
SOC_{ini}, SOC_{fin}	Initial and final SoC of energy exchange.
soc^{\min}, soc^{\max}	Minimum and maximum SoC.
sp_k	Speed of k-th EV.
s, m	Number of servers and customers.
$th^{wt}, th^{dt}, th^{ch}$	Threshold of waiting time, distance, and
	charging.
th^{cycle} , th^{EV}	Threshold of life cycle and BCS
	accessibility.
wt ^{max}	Maximum waiting time for all BCSs.
v_i, v^{\min}, v^{\max}	node i voltage, allowable minimum and
	maximum voltage.
X_i	A binary variable indicating whether <i>i</i> -th
chch	node should be deployed a BCS or not.
$egin{aligned} x_p^{ch}, x_q^{ch} \ x_p^{dch}, x_q^{dch} \end{aligned}$	Range anxiety parameter. Price sensitivity parameter in trading.
Δx Δx	Price's impact on range anxiety.
Δl , Δt	SoC level interval and time interval.
$\Delta soc_k^{ch}, \Delta soc_k^{dch}$	Change of SoC for charging and discharging.
$\Delta soc^{road}_{(j,j+1),k}$	Change of SoC driving from $r_{j,k}$ to $r_{j+1,k}$.
$\Delta t^{road}_{(j,j+1),k}$	Travelling time $r_{j,k}$ to $r_{j+1,k}$.
ΔE_k	Loss of exploitable energy of battery.
$\eta^{^{ch}}, \eta^{^{dch}}$	Efficiency of charging and discharging.
$\mu(t), \delta(t)$	Service and arrival rate at time <i>t</i> .
$\varepsilon(t)$	Probability of parking.
$\sigma(state^1, state^2)$	Transition probability of two states.
λ_{exp}	Expected price.

I. Introduction

ue to the rising awareness of environmental sustainability, the transportation system has been shifting from fuel-based vehicles to electric vehicles (EVs), and the power community has been devoted to accommodating more renewable energy sources (RESs) to construct a cleaner grid [1-3]. The concept, EV energy network (EVEN), developed from vehicle-to-grid (V2G), emphasizes on the EVs' transmission ability between rural RESs and urban user end [4]. EVEN has recently gained attention for its significant benefits, including smoothing RESs' utilization, supporting EV load, managing peak

demand, acting as the energy storage system, and offering drivers profits [5, 6].

Bidirectional charging station (BCS) is the key component in EVEN. Different from traditional unidirectional CS, it enables the reverse flow of energy from the vehicle to the grid. BCS deployment is of paramount importance for EVEN, providing the essential infrastructure to meet EV energy demands, directly affecting grid load dynamics and shaping the accessibility and utilization of RESs. A critical prerequisite for BCS deployment is the EV load prediction, as the spatial-temporal demand distribution dictates the siting and capacity of the BCSs. Additionally, it helps drivers to evaluate cost and profit, and enable operators to assess renewable energy consumption and develop financial auxiliary policies [7]. Notably, the major participants in our paper are public service EVs, such as bus, taxi, truck, and etc. The reasons are: (1) They are key players in EVEN, as they are constantly on the road during work hours, requiring and transmitting more energy. (2) Their extensive driving range enables them to deliver renewable energy to urban areas. (3) They have larger battery capacities, such as medium-sized EVs like buses and heavy-duty trucks. A 60 kW electric bus can power an electrically-heated home for 2 hours. Converting 1,000 gasoline buses to electric could supply energy to 24,000 homes for 2 hours [8]. (4) These drivers have free time. For example, Truck drivers can sell electricity in nearby CS during breaks. Instead of wasting time, they own more willingness for the participation.

Typically, there are two main approaches to obtaining EV load data: (dis)charging scheduling and driver behavior modelling. The former focuses on the strategic control of EV energy flow. This stems from researchers' interest in harnessing the potential of flexible and mobile EVs to enhance both economic efficiency and energy performance. The typical objectives of related works include: minimizing energy loss [6], energy consuming [9], economic cost [10], and maximizing total energy flow between energy plant to CS [11]. While modelling estimates electrical load under typical operating conditions. It focuses on the natural character of drivers without external intervention. In recent years, most of the EVEN-related research focuses on scheduling, drivers' behavior modelling is vacant in this field. From the perspective of BCS planner, relying on scheduling patterns is relatively unpractical for the following reasons: 1) The coexistence of multiple scheduling agents may result in deviations from planned outcomes. 2) Privacy concerns make it challenging for planners to accurately assess which scheduling strategies are in use and the corresponding share of EV users. 3) Drivers add further uncertainty, as individuals may switch energy management providers or even opt out of scheduled plan. Therefore, the second approach: modelling has been regarded as a more viable method for consideration. Most deployment works focus on stochastic load modelling, rather than scheduling [12-14].

Driver behaviour modelling can be classified into 3 categories: assumption-based method, data-driven method, and Markov method. Assumption-based method simplifies demand into designated mode by considering assumptions and

factors, including traffic flow [15], parking time [16], and etc. For discharging works, the assumptions are relatively unrealistic, such as fixed discharging location, time, and volume [17-20]. Also, these assumption-based methods simulate a homogeneous load, as it typically captures the macro-level aggregate load at specific locations without randomness. The second type, data-driven method is widely applied as it is straight-forward and easily to implement. Specifically, the relevant probability distributions are collected from real-world survey data, including arrival time, departure time, initial SoC, duration, and etc. Next, Monte Carlo method is employed to generate samples, enabling the load estimation [21, 22]. However, most of the data comes from internal combustion engine vehicles, which overlooks the EV specific features. Also, the individual behaviour cannot be adequately described and reasoned. The third type, Markov model is then introduced to tackle the above issues, which facilitates load prediction by probabilistically capturing the transitions between different states, including parking, driving, and charging [23-25]. However, distribution characteristics of behaviour-related parameters are not explicitly addressed in these studies, limiting the behaviour understanding and its application in deployment design. [26] proposed a general Markov charging model, which incorporates range anxietyrelated parameters and demonstrates the fitting ability for multiple real-world data. The feasibility of integrating price into the model is also validated. Nonetheless, discharging models remain underexplored in data-driven method and Markov method, with challenges in obtaining discharging data, and voids in designing discharging states. As V2G and renewable energy utilization are vital parts in EVEN, pricesensitive (dis)charging model is needed to further developed.

Corresponding to the vacant of discharging in load modelling, most deployment optimization studies focus on charging load, and few studies have addressed discharging profiles. In the future, discharge is nonnegligible for infrastructure planning for the following reasons [27]: 1) the discharge energy is considerable with numerous participants. Especially in the EVEN which provides the cheap and even free electricity from RESs, hence the spatial and temporal load pattern will be greatly changed. 2) If drivers choose to discharge at peak hours for higher profits, this may cause congestion, which is an important consideration evaluated as waiting time for planning. Therefore, further investigation of discharging and their impact on deployment is essential.

Moreover, EV energy storage devices greatly influence drivers' behavior and infrastructure deployment. The most common devices are battery and ultracapacitor. Batteries offer relatively high energy density, while ultracapacitors provide longer lifespans without degradation and higher (dis)charging rate [28, 29]. Higher energy density allows for greater capacity, longer life minimizes degradation costs, and higher rate enables faster energy transaction, all of which impact the EV load profile. Nevertheless, all the aforementioned articles assume a single battery for both travel and trading functions. In EVEN, frequent energy exchanges are required, and concerns about battery health may deter driver participation. trading scenarios with different device configurations can leverage the strengths of each equipment,

offering drivers and operators flexible, informed options for better outcomes. To the best of the authors' knowledge, the impact of varying device settings on driver behavior and deployment has not been addressed in the literature.

More specifically, the main contributions are:

- A novel general stochastic Markov (dis)charging model is proposed to capture dynamic spatiotemporal load patterns. The model is highly adaptable to various real-world factors, such as EV specification, electricity price, and battery level of charge. Drivers' personal characteristics are explicitly presented, including range anxiety, economic sensitivity, and decision execution. A parameter selection algorithm is newly designed to fit real-world charging data.
- A multi-objective BCS deployment strategy is presented. It targets at EV owners and grid operator with the consideration of minimizing driver's electricity cost and operator's installation cost, while ensuring voltage stability and quality of service, i.e., maximum waiting time and accessibility. To achieve this, a hybrid algorithm is developed. Based on the genetic algorithm (GA) framework, hill climbing (HC) is employed for further exploitation and particle swarm optimization (PSO) is for better evolvement with next generation. Also, the planning characteristics are utilized for revising initialization and mutation operators.
- Six different equipment configuration scenarios are studied, including (S1) no trade; (S2) trade in main battery; (S3) trade in extra battery; (S4) trade in extra ultracapacitor; (S5) trade in both main and extra battery; (S6) trade in both main battery and ultracapacitor. Main battery refers to the battery supporting EV driving. To the best of authors' knowledge, this is the first paper to explore behavior modelling and BCS deployment with diverse equipment settings in the context of EVEN. Our findings provide insights into selecting device configurations for both drivers and operators, validate financial policies for attracting EVs participation, and offer drivers with guidance on adjust their behavior for better profit while maintaining SoC.

Literature review is presented in Section II. Section III and IV introduce the theoretical background of drivers behavior model and BCS deployment method, respectively. Section V conducts a case study for the charging model. Section VI presents experiment for the BCS deployment and drivers' performance. A conclusion is drawn in Section VII.

II. LITERATURE REVIEW

Electric Vehicle Energy Network (EVEN). EVEN is proposed as an energy delivery system comprising EVs, BCSs, and the transportation network. Its fundamental concept is to transport energy from rural renewable energy plants to urban areas with high energy demand via EV fleet. In traditional electricity transmission via power lines, total energy losses can reach up to 30%, including a 10% loss from DC to AC conversion, 6.5% losses during transmission, and

		EV load prediction			BCS deployment					EVEN
Ref.			Considerations				Considerations			
KCI.	V2G	RES	Personal preference	Different trading devices	CS cost	EV cost	QoS (waiting time)	Grid stability	Method	
[12]	x	✓	✓	x	✓	✓	x	✓	MILP	x
[14]	×	x	x	x	✓	×	x	×	MILP	×
[15]	×	×	×	x	✓	×	√ M/M/s	×	RL	×
[16]	×	x	×	x	✓	\checkmark	√ M/M/s	×	Greedy	×
[17, 18]	✓	x	×	x	×	x	×	✓	Heuristic	×
[19]	✓	✓	×	x	✓	×	×	✓	MILP	✓
[20]	✓	✓	×	x	✓	×	×	×	Greedy	✓
[22]	×	×	✓	x	✓	×	✓ M/M/s	✓	Hybrid	×
[23]	×	×	✓	x	✓	×	√ M/M/s	×	-	×
[31]	×	✓	×	×	✓	×	x	×	Greedy	✓

TABLE I
SUMMARY AND COMPARISON OF LITERATURES

an additional 15% loss from AC to DC conversion. In contrast, utilizing electric vehicles (EVs) as mobile energy carriers can reduce these losses to around 10% largely due to the high charging and discharging efficiency of EV batteries, which is approximately 95% [20]. EVEN emerges as a pivotal component in advancing smart grid technologies and modernizing energy systems owning to the advancements and Energy Internet (EI) development. V2G enables bidirectional power exchange between electric vehicles and the grid. The worldwide market for V2G is expected to increase from \$11.3 million in 2023 to \$59.2 million by 2030 with an annual growth rate of 26.6% during this period [30]. EI fosters an intelligent, interconnected energy ecosystem, enhancing coordination among diverse energy resources. Besides the advantage of reducing energy loss, there are numerous benefits of EVEN: including augmenting the capacity of power grid, enhancing renewable energy utilization, mitigating the intermittency inherent in renewable generation, smoothing load profiles, reducing peakto-valley fluctuations, and providing additional income streams for vehicle owners [5, 6]. Several other similar architectures embody this basic concept under different nomenclatures, such as the electric vehicles energy internet [31], vehicular network [32], and vehicular energy network [4]. Recent studies of this area mainly focus on energy management. [6] designed an energy routing model for minimizing energy loss in time-varying vehicular networks. [10] optimizes energy allocation in localized energy networks. In [11], routing and dynamic storage for renewable energy are jointly optimized. [33] addresses route and (dis)charging scheduling to increase economic benefits for drivers. Another work focus on communication. [9] focuses on network selection and computation offloading in vehicular edge computing to reduce latency and energy consumption. These studies underscore the importance of utilizing renewable energy, positioning EVs as mobile storage, and enabling IoTbased intelligent (dis)charging interactions to support peak load management, renewable energy use, and energy loss reduction. However, significant EV participation is the prerequisite for above works, which in turn requires accessible and reliable infrastructure support. Unlike traditional deployment with unidirectional CS, BCS is requested in

EVEN, which allows V2G and hence impacts load dynamics significantly. There has been limited research on this topic, and the review is conducted in the next part.

Point queue

GA

GA

Drivers' behaviour Modelling and BCS Deployment in EVEN. Generally, CS deployment primarily focuses on determining optimal CS locations and capacities to meet increasing EV demand while constrained by limited resources considering human activity patterns. Studies mainly target three stakeholder perspectives, including CS planners, grid operators, and EV drivers. Grid-focused studies typically aim to minimize energy or power loss. [34] minimizes energy loss while considering voltage deviations, using MC simulations to form charging load but disregarding V2G. [17] and [18] concentrate on reducing power loss with voltage, current and power constraints. The discharging profiles are formed by predefining the number of V2G EVs at CS. [20] also targets energy loss with electric bus. The discharging is considered by defining hop, which means one time of charge and discharge during the regular route. From the angle of drivers, [15] maximizing quality of service (QoS), i.e., waiting time and range anxiety is often considered. [31] optimizes CS accessibility to RES without load prediction, since only site selection is discussed, ignoring capacity design. Apparently, single-objective approaches lack comprehensive analysis, prompting a shift toward multi-objective optimization. [16] considers deployment with driver and CS operator angle, such as charging likelihood, charging demand, and coverage of points of interest. [14] aims to minimize the electric bus purchasing fee, CS construction cost, and maximize environmental equity. [22] optimizes CS profits and QoS with elastic charging demand adjusted by waiting time and travelling distance. [35] minimizes both construction and travel costs with dynamic charging model, emphasizing traffic constraints for expressways. [19] targets operational cost and carbon emissions. To model discharging, authors assume that discharge begins at the end of final trip, start charging after discharge, and fully charge each time. Among these works, there are mainly three types of optimization algorithms are used, including exact calculation algorithm, the approximate approach, and hybrid algorithm. Exact calculation method, e.g., mixed integer linear problem, is able to find optimal solutions with commercial solvers, but is hard to solve nonlinear optimization with large-scale application [15]. Approximate approaches trade-off between solution optimality

100

and computational efficiency. They are particularly beneficial when addressing issues of complexity and scalability. Genetic algorithms and particle swarm optimization are the most prevalently utilized techniques. Hybrid approaches amalgamate various methods to harness their benefits, thereby they represent a promising strategy for formulating solutions [36].

The comparison with above studies is summarized in Table 1, highlighting the focus of our work. If the work considers V2G and RESs, it is assumed can be used in EVEN application. From the table, it can be concluded that: 1) Most works overlook the V2G, which is not applicable in BCS. 2) V2G-relevant studies employ over-simplified and unrealistic assumption, which limits applicability. 3) Deployment studies are designed from limited perspectives, and hybrid algorithm deserves further study; 4) Waiting time is often estimated based on constant load by M/M/s, which may fail to reflect the maximum waiting time. 5) None of the reviewed articles consider scenarios with different trading devices.

III. MARKOV-BASED DRIVER'S BEHAVIOR MODEL

Our model aims to depict (dis)charging behaviors across time and space. Electricity price is pre-determined and precommunicated to drivers.

A. States and Connections

States and their connections are deigned as in Fig.1. States are: charging c(l), discharging d(l), and running r(l), where land l' indicates SoC level of main battery and second device. Transitions with l are shown with solid lines, while others are dotted lines. There are 3 models. Model 1 is for the main battery without trading. Two states are r(l) and c(l). Charging raises the SoC, while driving lowers it, shown by rightward and leftward arrow. Model 2 is for main battery both for trading and driving. Discharging state is added, which also decreases SoC. Model 3 is for extra trading-only device, including battery or ultra-capacitor. Compared with model 2, running states are unconnected, as the second device does not consume energy. Specially, parking is represented by selfloops at r(l) without actions and energy variance. The probability is presented by $\varepsilon(t) \in [0, 1]$, which is a vector with the dimension equals to the number of time intervals. Table 2 concludes the relationships between the models and scenarios. The models for S3 and S4, as well as S5 and S6, are identical. Their differences arise in the use of battery or ultracapacitor.

B. Transition Probability

The probabilities are built by exponential-related sigmoid functions p(in) and q(in). In economics theory, the functions often model preferences, where risk aversion remains stable across preference levels [37]. In our case, the two main factors influencing behavior, i.e., price and SoC, vary with conditions, fitting the framework of state-dependent utility. The ability in drivers' behavior modelling has also been proved [38, 39].

$$p(in) = \frac{1}{1 + e^{-k_p(in - x_p)}}, \quad q(in) = \frac{1}{1 + e^{-k_q(-in + x_q)}}$$
(1)

Where *in* is the input, and x and k are adjustable parameters. For simple clarity, x represents both x_p and x_q , and k means k_p and k_q .

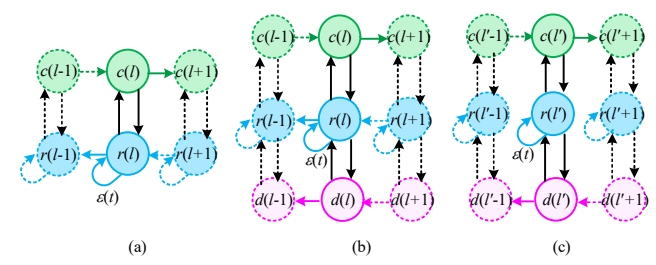
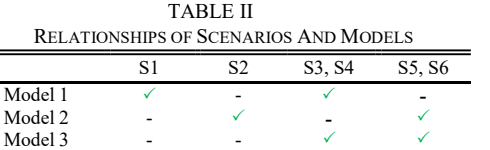


Fig. 1. Proposed stochastic (dis)charging model. (a) Model 1: main battery without trading. (b) Model 2: main battery both for trading and driving. (c) Model 3: extra device for trading.



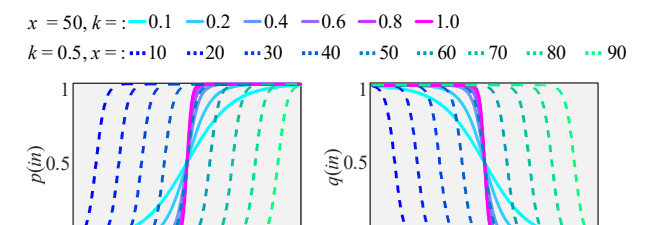


Fig. 2. p(in) and q(in) curves with k and x related parameters

100

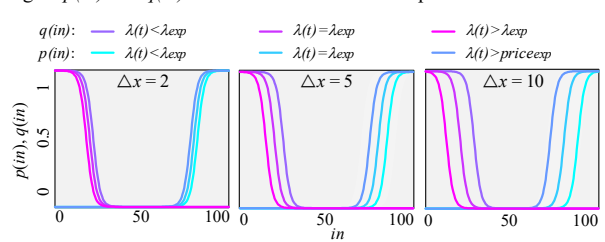


Fig. 3. p(in) and q(in) curves adjusted by different Δx

Fig. 2 visualizes p(in) and q(in) with different x and k. In charging or discharging context, the subscripts ch and dch are utilized. For charging, since drivers tend to start charging at low SoC and stop at high levels, their probabilities can be presented by q and p with SoC level l as in. For parameters, k influences its slope, while x shifts the curve horizontally. In terms of personal characteristic, k represents decisiveness. With k increases, the curve becomes steeper, suggesting a driver who are likely to make firm, binary decisions. x reflects range anxiety: larger x shifts both p(in) and q(in) to the right, so drivers tend to start charging at a higher SoC and stop until nearly full. In addition to inherent traits that contribute to driving anxiety, x is also influenced by real-time price: high cost has a suppressive effect, so price can be incorporated to adjust x. To start with, two boundaries should be set, the minimum $(x_q^{ch} - \Delta x, x_p^{ch} - \Delta x)$ and maximum $(x_q^{ch} + \Delta x, x_p^{ch} + \Delta x)$ willing to charge. Driver's willingnes will fluctuate between these two extremes, depending on the deviation between their expected price and the current price. If $\Delta x=0$, the change of price will not affect the charging behavior, so Δx reveals how much range anxiety can be affected by price. When renewable energy is available, drivers are most willing to charge. x_q^{ch} and x_p^{ch} can be obtained as:

$$\begin{cases} x_p^{ch}(\lambda) = \max \left\{ x_p^{ch} - \Delta x, x_p^{ch} - \Delta x \middle| \lambda - \lambda_{\exp} \middle| / 100 \right\} & \lambda > \lambda_{\exp} \\ x_p^{ch}(\lambda) = \min \left\{ x_p^{ch} + \Delta x, x_p^{ch} + \Delta x \middle| \lambda - \lambda_{\exp} \middle| / 100 \right\} & \lambda < \lambda_{\exp} \end{cases}$$
(2)

$$\begin{cases} x_q^{ch}(\lambda) = \max\{x_q^{ch} - \Delta x, x_q^{ch} - \Delta x \middle| \lambda - \lambda_{\exp} \middle| /100\} & \lambda > \lambda_{\exp} \\ x_q^{ch}(\lambda) = \min\{x_q^{ch} + \Delta x, x_q^{ch} + \Delta x \middle| \lambda - \lambda_{\exp} \middle| /100\} & \lambda \le \lambda_{\exp} \end{cases}$$
(3)

In Fig. 3, different Δx is visualized with maximum impact. Curves exhibit a larger shift with higher Δx . When the $\lambda < \lambda_{exp}$, curves move rightward, so drivers are likely to charge even without reaching a range-anxiety threshold. Hence

$$p^{ch}(l) = \frac{1}{1 + e^{-k_p(l - x_p^{ch}(\lambda))}}, \quad q^{ch}(l) = \frac{1}{1 + e^{-k_q(-l + x_q^{ch}(\lambda))}}$$
(4)

For discharging, since drivers are likely to discharge when prices are high and stop when prices drop, so the probabilities are p and q with the λ input. k indicates decisiveness, while x reflects price sensitivity. A higher x suggests a preference for discharging only at high prices and stopping at minor price dips, placing greater emphasis on economic returns. When l=0, there is no energy, so $p^{dch}(\lambda)$ =0, and $q^{dch}(\lambda)$ =1.

$$p^{dch}(\lambda) = \frac{1}{1 + e^{-k_p(\lambda - x_p^{dch})}}, \quad q^{dch}(\lambda) = \frac{1}{1 + e^{-k_q(-\lambda + x_q^{dch})}}$$
 (5)

Based on above p and q related probabilities, the transient probability $\sigma(state^1,state^2)$ in models are summarized as Table 3. Their calculations all adhere to *Principle* 1, which is also used in [24].

Principle 1: For a given state *state*¹, if there are *Ns* possible transitions, then the sum of all transition probabilities equals 1.

$$\sum_{ns=1}^{Ns} \sigma(state^1, state^{ns}) = 1$$
 (6)

Model 1 [26]: For state r(l), $\sigma(r(l), r(l))$: As self-loop of r(l) represents parking, so it is $\varepsilon(t)$. $\sigma(r(l), c(l))$: two events happen, i.e., no parking $1-\varepsilon(t)$ and deciding to charge $q^{ch}(l)$, so the probability is the multiplication, and $\sigma(r(l), r(l-1))$ is obtained by *principle* 1. For c(l), drivers tend to stop charging with $p^{ch}(l)$ as $\sigma(c(l), r(l))$, while $1-p^{ch}(l)$ to continue as $\sigma(c(l), c(l+1))$.

Model 2: Compared with model 1. discharging d(l) is newly added. For discharging related transient, $\sigma(r(l), d(l))$: three events are happened, i.e., no parking $1-\varepsilon(t)$, abundant energy $1-q^{ch}(l-\Delta l)$, and deciding to discharge $p^{dch}(\lambda)$, where $\Delta l > 0$. $\sigma(r(l), r(l-1))$ is also obtained by 1 minus remaining probabilities. For $\sigma(d(l), d(l-1))$, abundant energy $1-q^{ch}(l-\Delta l)$ and not to decide stop charging $(1-q^{dch}(\lambda))$ are considered.

Model 3: There are no links between running states since no energy is consumed by driving. Two sets of p and q are applied, i.e., $q^{dch}(\lambda)/p^{dch}(\lambda)$ and $q'^{dch}(\lambda)/p'^{dch}(\lambda)$. Their differences are in x. The conditions, $x'_{q}^{dch} > x_{q}^{dch}$ and $x'_{p}^{dch} > x_{p}^{dch}$ with the difference of Δx^{dch} , ensure profitability. For $\sigma(r(l), d(l))$, two events are no parking $1-\varepsilon(t)$ and deciding to discharge $p'^{dch}(\lambda)$. $\sigma(r(l), c(l))$ is calculated by $(1-\varepsilon(t))$ and $q^{dch}(\lambda)$. Other probabilities are calculated at the same way.

C. Models in Trading Scenarios

This part explains how to implement above models in six trading scenarios with road network, BCS locations, RESs, etc. Assuming drivers are served once arriving. calculations are shown in Fig. 4. Remaining energy at the destination is

$$e_{i,k}^{remain} = soc_{i,k} \cdot cap_k - dt(r_{i,k}, r_{des,k}) \cdot e_k^{consume}$$
 (7)

TABLE III
TRANSIENT PROBABILITIES IN MODEL 1, 2, AND 3

	KANSIENT I KOI	BABILITIES IN MODEL 1	, 2, AND 3
Probability	Model 1	Model 2	Model 3
$\sigma(c(l), r(l))$	$p^{ch}(l)$	$p^{ch}(l)$	$p^{dch}(\lambda)$
$\sigma(c(l), c$	$1 - p^{ch}(l)$	$1 - p^{ch}(l)$	$1 - p^{dch}(\lambda)$
(l+1))			
$\sigma(r(l), r(l))$	$\mathcal{E}(t)$	$\varepsilon(t)$	$1-(1-\varepsilon(t))(q^{dch}$
			$(\lambda)+ p^{\prime dch}(\lambda))$
$\sigma(r(l), r(l-1))$	$(1-\varepsilon(t))(1-$	$(1-\varepsilon(t))(1-q^{ch}(l)-(1-$	-
	$q^{ch}(l)$	$q^{ch}(l-\Delta l)) p^{dch}(\lambda))$	
$\sigma(r(l), c(l))$	$(1-\varepsilon(t))q^{ch}(l)$	$(1-\varepsilon(t))q^{ch}(l)$	$(1-\varepsilon(t))q^{dch}(\lambda)$
$\sigma(r(l), d(l))$	-	$(1-\varepsilon(t))(1-q^{ch}(l-\Delta l))$	$(1-\varepsilon(t)) p^{*dch}(\lambda)$
		$p^{dch}(\lambda)$	
$\sigma(d(l), r(l))$	-	$q^{dch}(\lambda)+q^{ch}(l-\Delta l)$ -	$q^{\prime dch}(\lambda)$
		$q^{dch}(\lambda)q^{ch}(l-\Delta l)$	
$\sigma(d(l), d(l-1))$	-	$(1-q^{dch}(\lambda))(1-q^{ch}(l-$	$1-q^{\prime dch}(\lambda)$
		$\Delta l))$	

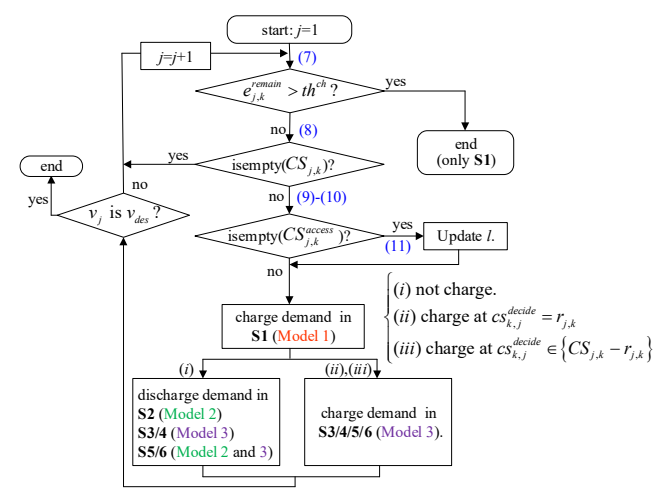


Fig. 4. (Dis)charging demand calculation of 6 scenarios by 3 models

If remaining energy is higher than the threshold, meaning is sufficient, the procedure ends in S1. Next, $CS_{j,k}$ yields

$$CS_{j,k} = \left\{ r_i \mid dt(r_{j,k}, r_i) \le th^{dt}, r_i \in CS \right\}$$
 (8)

If $CS_{j,k}$ is empty, EV goes to the next node. $CS_{j,k}^{access}$ is

$$dt_{i,k}^{\max} = soc_{i,k} \cdot cap_k / e^{consume}$$
 (9)

$$CS_{j,k}^{access} = \left\{ r_i \mid dt(r_{j,k}, r_i) \le dt_{j,k}^{\max}, r_i \in CS \right\} - CS_{j,k}$$
 (10)

If $CS_{j,k}^{access}$ is empty, meaning there is no chance to charge after $r_{j,k}$, so SoC can be updated

$$soc_{j,k}^{remain} = e_{j,k}^{remain} / cap_k$$
 (11)

Charging behavior in S1 is decided by model 1. For BCS with available renewable energy, free greatly enhances $q^{ch}(l)$ and motivates drivers to charge. However, due to the intermittency and variability of RES, its output may not align with EV demand. When a large number of EVs approaches, their charging requirement may exceed the generation. In this condition, first-come first-served principle is applied. There are three possible results. First, no charge, so the driver would go to $r_{i+1,k}$. Second, charge at $r_{i,k}$, meaning $x_i=1$, and the charging energy and duration are decided by $\sigma(c(l), r(l))$. Third, charge at near node: charging is urgently needed but $x_i=0$, so the driver has to change the route to reach the nearest BCS. The trading is developed based on the above results. No charging means that SoC is relatively sufficient, or the price is high, so discharging of S2 to S6 are decided afterwards. S2 and S3/4 are based on model 2 or 3, respectively. Specially, in S5/6 two models are involved. In our work, trading first occurs in the second device if there is energy, which is calculated by model 3. If it is depleted, model 2 is utilized to calculate discharging in main battery. Charging indicates that the price might be attractive, so the charging of second device in S3 to S6 is modelled afterwards. The changes of SoC is

$$\Delta soc_k^{ch} = rt_k^{ch} \Delta t / cap_k \tag{12}$$

$$\Delta soc_{k}^{dch} = -rt_{k}^{dch} \Delta t / cap_{k} \tag{13}$$

$$\Delta soc_{k}^{dch} = -rt_{k}^{dch} \Delta t / cap_{k}$$

$$\Delta soc_{(j,j+1),k}^{road} = -dt(r_{j,k}, r_{j+1,k}) e_{k}^{consume} / cap_{k}$$

$$(13)$$

which are for charging, discharging and reaching the next node. The time consumed between the adjacent nodes can be expressed as

$$\Delta t_{(j,j+1),k}^{road} = dt(r_{j,k}, r_{j+1,k})/sp_k \tag{15}$$

The power demand can be calculated based on the change of SoC in the corresponding time. The profiles can be obtained as

$$pf^{ch}(t) = \sum_{n=0}^{\infty} \sum_{k=0}^{\infty} pf_{j,k}^{ch}(t) / \eta^{ch}$$
 (16)

$$pf^{ch}(t) = \sum_{R_k \in R} \sum_{r_{j,k} \in R_k} pf_{j,k}^{ch}(t) / \eta^{ch}$$

$$pf^{dch}(t) = \eta^{dch} \sum_{R_k \in R} \sum_{r_{j,k} \in R_k} pf_{j,k}^{dch}(t)$$
(16)

The simplified battery degradation model in [40] is given as

$$\Delta E_k \cong k_w cap_k \left| soc_{ini} - soc_{fin} \right| \tag{18}$$

where k_w is degradation-related parameter chosen as 0.00015. The degradation cost is calculated as

$$cap_k = cap_k - \Delta E_k \tag{19}$$

$$cost_{\iota}^{degrad} = (cap_{\iota}^{int} - cap_{\iota})cost_{\iota}^{b} / th^{cycle} cap_{\iota}^{int}$$
 (20)

D. Parameter Selection Algorithm

The algorithm is for $\varepsilon(t)$. Compared with other parameters, $\varepsilon(t)$ is high dimensional and plays a key role in fitting. The main idea of the algorithm is that higher $\varepsilon(t)$ increases the probability of no (dis)charging at a t. Therefore, $\varepsilon(t)$ is updated based on the error between the prediction and real data. In Algorithm 1, firstly, initialize and form a predicted profile. Then, calculate subtraction for each time segment and obtain the adjusting index. Specifically, if $\varepsilon(t)=1$ and sign>0, indicating that the predicted data is higher than the real data, $\varepsilon(t)$ should be increased but reach the upper limit, so it is nonadjustable. Next, update $\varepsilon(t)$ using step and sign, if the current sign differs from that of former iteration, the index scales by a decay weight. The selection stops when there is no adjusting index or at the end of cycles. Other parameters in our paper are decided by grid search approach. Also, the related parameters can be defined by driver as they are highly related to their personal characteristic.

E. Sensitivity Analysis

Fig. 5 visualizes the transient probabilities in Table 3, both complementarity and symmetry are clearly Complementarity, as introduced by Principle 1, results in a light-dark contrast, while symmetry emerges from the q and p curves due to their opposing input signs. Typical probabilities are explained in detail, including $\sigma(c(l), r(l))$ in model 1, $\sigma(r(l), r(l))$ d(l) in model 2, and $\sigma(c(l), r(l))$ in model 3, since other probabilities can be analyzed similarly using complementarity and symmetry. In model 1, $\sigma(c(l), r(l)) = p^{ch}(l)$. Larger difference between l and $x_p^{ch}(\lambda)$ brings the probability closer to

Algorithm 1 Parameter Selection Algorithm for $\varepsilon(t)$

Input: Real EV load profile $pf_r(t)$, probabilities $p^{ch}(t,l)$, $q^{ch}(t,l)$, decay weight w_{decay} , number of circles n_{cir} and other inputs for charging modeling. **Output:** Probabilities of parking in each time segments $\varepsilon(t)$.

- 1: Initialize the $\varepsilon(t)$ and the update step $step_{up}$. The number of time segments is n_t 2: Run the model to obtain the predicted load profile $pf_p(t)$ and $s_{pr}^1(t)$
- $s_{pr}^{1}(t) = sign(pf_{p}(t) pf_{r}(t))$
- for $i = 2:1:n_{cir}$ do
- Run the charging model based on above inputs, obtain $pf_p(t)$.
- $s_{pr}^{i}(t) = sign(pf_{p}(t) pf_{r}(t)); idct(t) = (\sum_{t=1}^{n_{t}} |pf_{p}(t) pf_{r}(t)|)/n_{t}$
- $\begin{array}{l} idx_{posi} = find(s_{pr} > 0), idx_{nega} = find(s_{pr} < 0) \\ idx_{adj} = [1:1:n_t] [find(\varepsilon(idx_{posi}) == 1)] [find(\varepsilon(idx_{nega}) == [find(idct(t) < th^{idct})] \end{array}$
- if $isempty(idx_{adj})$ then
- 10: return $\varepsilon(t)$.
- 11:
- 12:
- 13:
- $\begin{array}{l} \varepsilon(\mathrm{idx}_{adj}) = \varepsilon(\mathrm{idx}_{adj}) + s_{pr}(idx_{adj}) \cdot \mathrm{step}_{up}(idx_{adj}) \\ idx_{decay} = \mathrm{find} \ (s^{i-1}_{\ pr}(t) \neq s^{i}_{pr}(t)) \\ step_{up}(idx_{decay}) = w_{decay} \cdot \mathrm{step}_{up}(idx_{decay}) \end{array}$ 14:
- end if 15:
- 16: end for



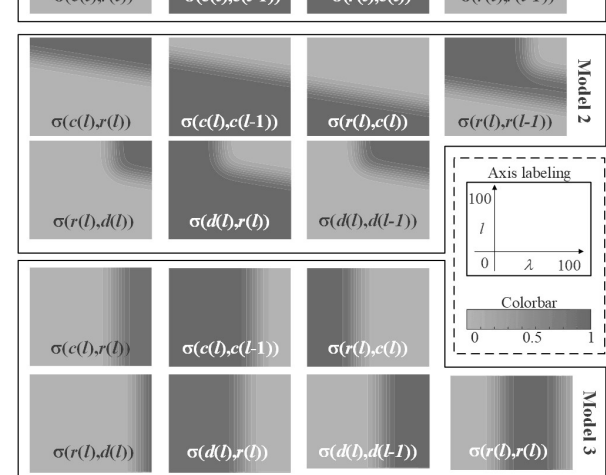


Fig. 5. Transient probabilities with x axis of λ and y axis of $l: k=0.2, x_p^{ch}=x$ =70, $x_q^{ch} = x_q^{dch} = 40$, $\lambda_{exp} = 50$, $\Delta x = 10$, $\Delta l = \Delta \lambda = 20$.

1. For fixed λ , the high-probability region is concentrated in the upper area. While for fixed l, larger λ decreases $x_p^{ch}(\lambda)$, resulting in a dark triangular shape in the upper right. Complementarity is seen in $\sigma(c(l), c(l+1)) = 1 - \sigma(c(l), r(l))$, and symmetry appears in $\sigma(r(l), c(l)) = q^{ch}(l)$. In a charging context, lower SoC increases charging probability, while higher prices decrease it, and vice versa. In model 2, $\sigma(r(l))$ $d(l) = (1-q^{ch}(l-\Delta l)) p^{dch}(\lambda)$. The first term parallels $\sigma(r(l), r(l-\Delta l))$ 1)) in model 1, but with a reduced area due to Δl . The second term, influenced by λ , creates a left-bright, right-dark region, causing a penumbra-like shape in the upper-right corner. Here, higher SoC and prices encourage discharging, with the price acceptance range set by $x_{dch}^q < x_{dch}^p$. In model 3, $\sigma(c(l), r(l)) =$ $p^{dch}(\lambda)$. Unlike model 1, is independent of l due to a constant x^{ch} , forming a square-shaped dark area on the right. For above discussion, transitions governed by complementarity and symmetry indicate a balanced process in which state probabilities dynamically adjust based on behavior-related parameters, capturing nuanced changes across models.

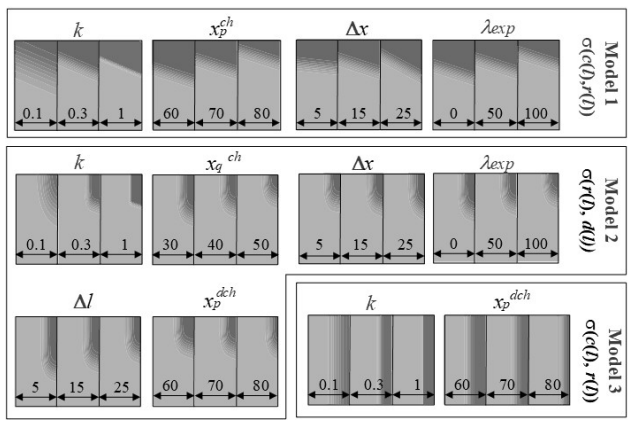


Fig. 6. Sensitivity analysis of selected transient probability with x axis of λ and y axis of l.

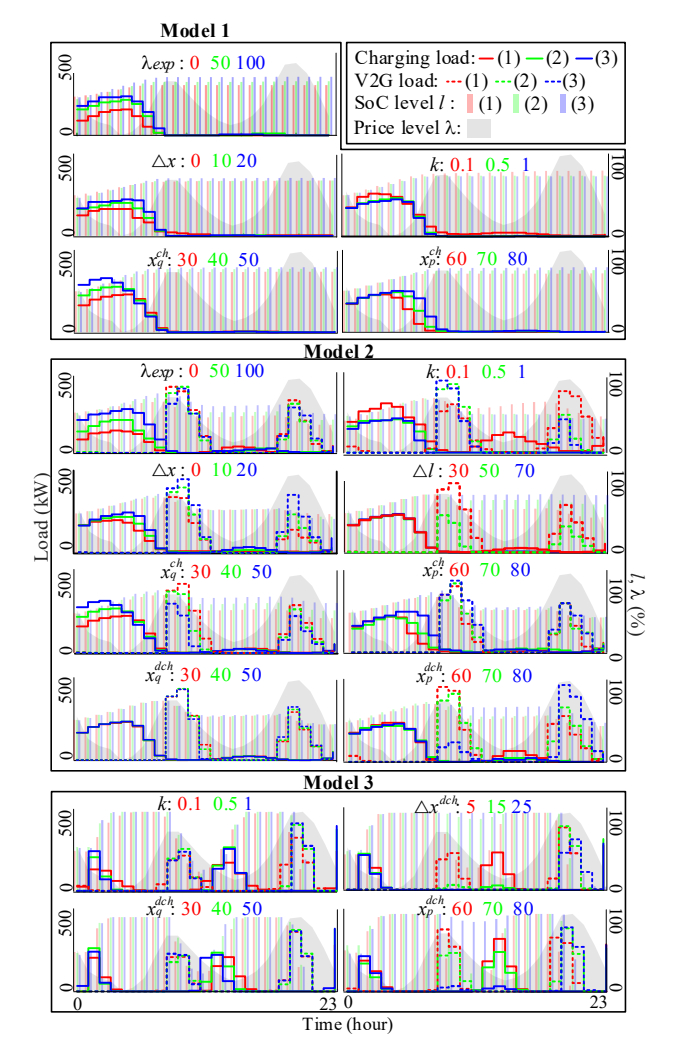


Fig. 7. Load of 3 models under different parameters

Next, the sensitivity analysis of above probabilities is presented in Fig. 6, using the same axis labels and color bar as Fig. 5. k controls steepness. A larger k sharpens the light-dark boundary across all models, indicating 0-1 probability action for drivers. For x_p^{ch} and x_q^{ch} , higher values represent increased range anxiety, shifting the dark region upward in models 1 and 2. Δx reflets the impact of electricity price on range anxiety, expanding the range of $x_p^{ch}(t)$ and $x_q^{ch}(t)$. This appears as a steeper triangular slope in model 1 and a downward extension of shading in model 2. λ_{exp} , as the price threshold, shifts the shaded area upward in models 1 and 2. Δl , defining the safe discharging SoC range, enforces stricter limits on l, visualized as an upward shading shift in model 2. x_p^{dch} , associated with discharging initiation, increases the high-probability region's rightward movement in models 2 and 3 with higher values. Therefore, by adjusting these parameters, distinct driver behaviors are effectively characterized within the model.

The effects on (dis)charging load across the 3 models are analyzed using 100 EVs with 60 kWh battery capacities, initialized at 00:00 with a power rate of 6 kW. In Fig. 7, 3 values are selected, with solid and dashed lines representing the load curves for charging and discharging, and bars showing the 24-hour average SoC. The shaded area indicates 24-hour price fluctuations, scaled to 101 levels to correspond to λ . For λ_{exp} in model 1 and 2, an increase raises the charging load due to a higher price acceptance threshold. As expected prices rise, discharging decreases, hence increases SoC. For Δx in model 1 and 2, higher values elevate the load with a slight delay as drivers opt to charge during low-price intervals. Higher x_p^{ch} and x_q^{ch} reveal drivers' preference for early charging initiation and delayed cessation due to driving anxiety, and higher x_q^{ch} further suppresses discharging, which are shown in model 1 and 2. For Δl in model 2, the safety margin is adjusted adversely. Only discharging is affected, and discharging ceases entirely with value of 70. x_p^{dch} and x_q^{dch} is positively related to strict price requirements. Higher x_p^{dch} delays discharging until prices are elevated, and charging load decreases as the high-probability region of $\sigma(r(l), c(l))$ is surpressed. In model 3, larger Δx^{dch} intensifies trading in highprice-difference zones. Lastly, a large k reduces randomness, with inherent behaviors primarily guided by other parameters. Thus, the impact on load corresponds and relates directly to changes in transient probabilities. Parameter adjustments allow targeted control over EV (dis)charging patterns, with distinct behaviors emerging in response to price sensitivity, range anxiety, execution ability, and safety margins across the models.

IV. BIDIRECTIONAL CHARGING STATION DEPLOYMENT

A. Optimization Formulation

1) Objective Function. The goal is to maximize score:.

$$score = 1/(w_1 cost^{operator} + w_2 cost^{driver})$$
 (21)

The operator cost is calculated by two parts, cost for constructing one BCS and cost for installing servers:

$$cost^{operator} = cost^{CS} \sum_{i \in V} x_i + \sum_{i \in V} x_i n_i cost^{server}$$
 (22)

Expenses for drivers consist of three parts: costelec, profit^{trade} and cost^{degrad}:

$$cost^{elec} = \sum_{t} pf^{ch}(t)price(t)\Delta t$$
 (23)

$$profit^{trade} = \sum pf^{dch}(t)price(t)\Delta t$$
 (24)

$$cost^{degrad} = \sum_{i} cost_{k}^{degrad}$$
 (25)

$$profit^{trade} = \sum_{t} pf^{dch}(t)price(t)\Delta t$$

$$cost^{degrad} = \sum_{k} cost_{k}^{degrad}$$

$$cost^{driver} = \left(cost^{elec} + cost^{degrad} - profit^{trade}\right) / \sum_{t} pf^{ch}(t)\Delta t$$
(24)

2) QoS Constraints. Firstly, most drivers can reach BCS within a certain distance along their route. If there is any close-range BCS through R_k , then $flag_k^{cs}=1$, which is given by

$$flag_k^{CS} = \begin{cases} 1, & for \ \forall r_{j,k} \in R_k, \ \exists CS_{j,k} \neq \emptyset \\ 0, & \text{o.w.} \end{cases}$$
 (27)

The constraint can be written as
$$pro^{pass} = \frac{\sum_{R_k \in R} flag_k^{CS}}{|R_k|} \ge th^{EV}$$
(28)

where $|R_k|$ is the total number of routes. It confirms at least one BCS close to the route. Secondly, the maximum waiting time is acceptable as described by

$$wt^{\max} \le th^{wt} \tag{29}$$

M(t)/M(t)/s model is employed to estimate wt^{max} [41] as (30)-(32). It is a time-varying queueing system where arrivals and service rates are both time-dependent, following Poisson processes. In the interaction of EVs and BCSs, M(t), M(t), and s represent EV demand (the arrival rate), the (dis)charging rate (the service rate), and the number of chargers (servers).

$$prob_0'(t) = -\delta(t) prob_0(t) + \mu(t) prob_1(t)$$
(30)

$$prob'_{m}(t) = -(\delta(t) + m\mu(t))prob_{m}(t) + \delta(t)prob_{m-1}(t) + (m+1)\mu(t)prob_{m+1}(t), \text{ if } 0 < m < s$$
(31)

$$prob'_{m}(t) = -(\delta(t) + s\mu(t))prob_{m}(t) + \delta(t)prob_{m-1}(t)$$
$$+s\mu(t)prob_{m+1}(t), \quad \text{if } m \ge s$$
(32)

The arrival rate is the sum of the EV load demand in the BCS as given by

$$\delta(t) = p f_b^{ch}(t) + p f_b^{dch}(t) + \left(p f_u^{ch}(t) + p f_u^{dch}(t) \right) r t_b / r t_u$$
 (33)

where subscripts u and b denote ultracapacitor and battery. Specially, since the (dis)charging rates of battery and ultracapacitor are different. The waiting time can be estimated by

$$wt(t) = \left(\frac{\sum_{m=s}^{m^{\max}} (m-s+1) \operatorname{prob}_{m}(t)}{s\mu(t)}\right) / s\mu(t)$$
 (34)

Different from our work, lots of works estimate system delay by M/M/s [15, 16, 22, 23], which assumes a constant arrival rate for system with steady-state conditions. In Fig. 8, two models are compared: the purple area indicates the timevarying EV demand, while the blue area represents the constant mean value. Observing the solid and dashed blue lines shows that, with an averaged input, both models' delays converge to the same value. Comparing the solid purple and blue lines reveals that M(t)/M(t)/s calculated delay exhibits a sinusoidal pattern, whereas M/M/s yields a constant value. Ensuring QoS requires keeping system delay within the limit. However, M/M/s significantly underestimates peak delay compared to M(t)/M(t)/s with a 41.7% relative error in this case, which is insufficient for QoS. Thus, it is concluded that M(t)/M(t)/s is more applicable for dynamic EV-BCS interaction system with time-varying EV load to maintain QoS.

3) Grid Constraints. The constriants with grid stability are:

$$P_{i}^{gen} - P_{i}^{bus} = \sum_{i'=1}^{N^{bus}} |v_{i}| |v_{i'}| (G_{ii'} \cos \theta_{ii'} + B_{ii'} \sin \theta_{ii'})$$
 (35)

$$Q_{i}^{gen} - Q_{i}^{bus} = \sum_{i'=1}^{N^{bus}} |v_{i}| |v_{i'}| (G_{ii'} \sin \theta_{ii'} - B_{ii'} \cos \theta_{ii'})$$
 (36)

$$P_{i}^{bus} = p f_{i}^{load}(t) + p f_{i}^{ch}(t) - p f_{i}^{dch}(t)$$

$$v^{min} \le v_{i} \le v^{max}$$
(38)

$$v^{\min} \le v_i \le v^{\max} \tag{38}$$

Time varying arrival rate $\sigma(t) = 3 + 2\sin(2\pi t)$ — M(t)/M(t)/s with $\sigma(t)$ Mean arrival rate $\sigma = \text{mean}(\sigma(t)) - M(t)/M(t)/s$ with $\sigma - M/M/s$ with σ

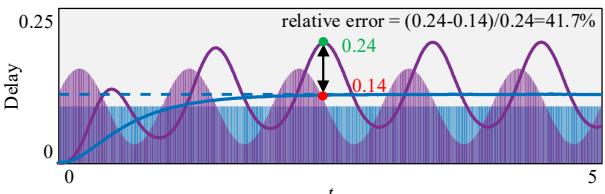


Fig. 8. Delay calculation by M(t)/M(t)/s and M/M/s with time varying arrival rate or constant mean arrival rate.

4) Other Constraints. The maximum number of servers is limited by (39); the SoC-related constraints are (40).

$$1 \le n_i \le n_{\text{max}}, \text{ if } x_i = 1$$
 (39)

$$soc^{min} \le soc_{\iota}(t) \le soc^{max}$$
 (40)

B. The Proposed Hybrid Algorithm

Our algorithm based on genetic algorithm (GA) framework. GA is searching techniques based on the process of natural selection. Evolutionary is simulated by working with a population of potential solutions that evolve through iterative processes. Fitness determines the quality of each solution, with more successful individuals having a higher chance of contributing to subsequent generations. GA owns the advantages of strong global search capability and high robustness. Also, its modular design provides flexibility of customizability. In GA, the next generation is created through crossover and mutation operators, which combine gene segments from parent solutions. However, crossover is inherently a global operation, lacking the ability to explore in the vicinity of local optima. Also, the randomness results in a lack of meaningful guidance for forming next generation, reducing the efficiency of evolution. Therefore, to address exploitation, hill climbing (HC) is introduced, which is a local search algorithm that iteratively improves solutions within the neighborhood of the current solution to find a local optimum. To imrove directional evolution, particle swarm optimization (PSO) is incorporated. The crossover is enhanced by leveraging both individual historical experience and collective knowledge of the population. Through velocity and position updates, the solution space is dynamically explored, avoiding inefficient searches cause by random gene recombination, hence the updates become more directional and continuous, accelerating the convergence. The success of the improvement crossover by PSO has been recognized [42]. The specific steps are as follow:

1) Initialization. Generation of random initial population. propass is considered for the improvement. The core idea is to mandatorily select nodes with a high traffic volume for construction. By assuming BCS is set at i-th node in turn, calculate $flag_k^{CS}$ by (27), hence n_i^{flag} is as (41). Sort n_i^{flag} for potential nodes in descending order to identify the top n^{CS} nodes as mandatory nodes. Also, constraint (39) is considered in the initialization phase. $n_i^{flag} = \sum_{R_k} flag_k^{CS}$

$$n_i^{flag} = \sum_{R} flag_k^{CS}$$
 (41)

2) Selection. Calculation of fitness to select individual. QoS constraint is addressed by penalty method. The basic idea is to incorporate a penalty term into the objective function that discourages solutions violating the constraints. The fitness score is updated by (42), where w_1^p and w_2^p is penalty weights. Higher score means greater probability of being selected.

$$score = score - w_1^p \max \left\{ 0, wt^{\max} - th^{wt} \right\}$$

$$- w_2^p \max \left\{ 0, pro^{pass} - th^{EV} \right\}$$

$$(42)$$

3) Offspring generation. Forming new offspring is divided into four groups. a) Crossover and mutation. high-scoring individuals are selected and mutated following traditional GA; b) Elite preservation. High-scoring individuals are retained to maintain good solutions; c) Constraint-directed adjustment. High-scoring individuals serve as templates, fine-tuning server numbers by comparing the maximum waiting time to the thresholds. d) Hill climbing. Solutions are refined through local searching and movement with best individual. Next, an offspring enhancement phase using PSO strategy is included. Based on equations of updating velocity and position, each particle is improved the population's convergence towards optimal solutions. Finally, the new offspring is obtained and the best solution is recorded for new iteration.

V. CASE STUDY: FITTING ABILITY FOR CHARGING BEHAVIOR

A. Case Description

Two data-sets used to validate the fitting ability of charging behavior in S1, which are online data-set from [43] and [44]. The number of EVs is 2000. The average speed is set as 40 km/h, and the energy consumed is 0.6 kWh/km [45]; the battery capacity is 80 kWh. The route is generated by the shortest path method. The departure time is formed by the probability distribution in [46]. The price is from [47].

B. Fitting Results

The selected parameters for two datasets are listed in Table 4. Prediction performance is evaluated by mean absolute percentage error (MAPE), mean squared error (MSE), and root mean squared error (RMSE) [26]. To avoid contingency, the model runs 50 times, and the curves and indicators are calculated by averaging the 50 random load profiles.

Firstly, the results of different $\varepsilon(t)$ dimension are visualized in Fig. 9. Grid search (GS) method is used with 0.1 search interval. Gray bars represent the collected EV charging load from the dataset. For dataset 1, peak is around 12:00, whereas in dataset 2, load peak is at approximately 9:00 and 10:00. Fig. 9 indicates that with the dimension of 24, our model fits well in both cases. As dimensionality reduces, the fit quality decreases. Also, it is clear that our model outperforms GS method. From Table 5, it is clear that higher dimensions improve 3 indicators. At dimension of 24, the optimal MAPE, MSE, and RMSE are achieved: 11.5%, 0.1%, and 3.6% for dataset 1, and 12.6%, 0.4%, and 6.5% in dataset 2. The superiority of our method over GS is demonstrated. Also, the proposed method is notably more efficient than GS. Higher dimension in our model will not affect efficiency, even ends faster, because requirements are meet more easily, hence ending the iteration earlier.

Next, three baseline methods are selected for comparison. [48], [49] are probability-distribution-based methods, while [26] is Markov-based method. Each method's probability distribution aligns with that in its original paper, including SoC, arrival, and departure distributions, and etc. Fitting for

TABLE IV PARAMETER SELECTION RESULTS

	x_p^{ch} , x_q^{ch} , k , Δx	$\mathcal{E}(t)$
Dataset 1	80, 30, 0.5, 3	[1.0,0.7,0.3,0.5,0.4,0.1,0.0,0.4,0.9,0.2,1.0,0.9, 0.8,0.8,1.0,0.9,0.9,1.0,0.9,0.9,1.0,0.9,0.9,0.9]
Dataset 2	80, 40, 0.5, 10	[1.0,1.0,1.0,0.9,0.9,0.1,0.1,0.1,0.3,0.9,0.8,0.9, 0.9,0.9,0.9,0.9,0.9,0.9,0.9,1.0,1.0,1.0,1.0]

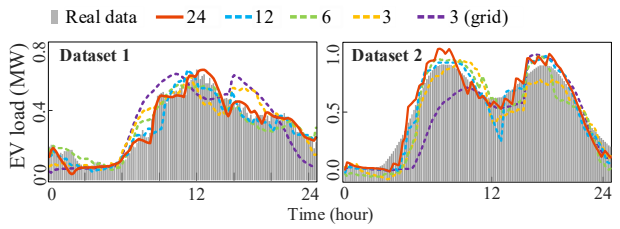


Fig. 9. Fitting result of different $\varepsilon(t)$ dimension of two data-sets.

TABLE V INDICATORS OF DIFFERENT DIMENSION OF $\mathcal{L}(t)$

Dimen	sion of $\mathcal{E}(t)$	3 (GS)	3	6	12	24
MAPE	Dataset 1	33.0	28.6	16.9	14.8	11.5
(%)	Dataset 2	24.0	18.8	16.4	15.9	12.6
MSE	Dataset 1	1.1	0.8	0.2	0.2	0.1
(%)	Dataset 2	1.6	1.6	1.2	0.8	0.4
RMSE	Dataset 1	10.4	8.6	5.0	4.4	3.6
(%)	Dataset 2	12.8	12.6	11.0	9.1	6.5
T	ime (s)	4009.7	433.8	428.7	380.7	380.4

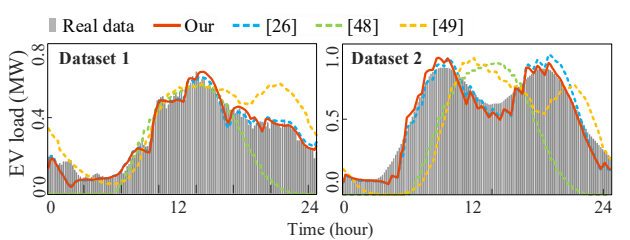


Fig. 10. Fitting result of different models of two data-sets.

TABLE VI INDICATORS OF DIFFERENT METHODS

-	Me	ethod	[48]	[49]	[26]	Our
_	MAPE	Dataset 1	53.6	29.7	11.8	11.5
	(%)	Dataset 2	65.0	40.9	14.4	12.6
	MSE	Dataset 1	2.4	0.9	0.1	0.1
	(%)	Dataset 2	12.2	7.1	0.4	0.4
	RMSE	Dataset 1	15.5	9.5	3.6	3.6
	(%)	Dataset 2	34.9	26.1	6.0	6.5

probability-driven methods is achieved by fine-tuning parameters such as capacity and charging rate, while the Markov method uses the same parameter selection approach as the proposed method. Fig. 10 visualizes the comparisons, with indicators in Table 6. The proposed method and [26] achieve the good fit for both datasets. Probability-driven methods show limited fitting ability. For instance, [48] forms a Gaussian-like curve, capturing the peak but missing intervals (00:00-06:00 and 22:00-24:00). It achieves relatively acceptable performance for dataset 1, while for dataset 2 the fitting is not satisfactory. Thus, [49] also cover the 24-hour load but lack fitting flexibility. Given probability distributions, the shape of the load curve is largely determined, restricting fitting performance. Indicators in Table 6 confirm our method achieves the best MAPE, with MSE and RMSE comparable to [26]. Therefore, the fitting ability of Markov-based models are demonstrated. Our method outperforms [26] as it can be extended to broader trading scenarios.

VI. CASE STUDY: BIDIRECTIONAL CHARGING STATION DEPLOYMENT

A. Case Description

In Fig. 11, the road network is a 6×5 grid with 177 nodes, labelled as i for clarify. The red line illustrates R_1 , which contains $r_{1,1}$, $r_{2,1}$, and $r_{3,1}$. These correspond to nodes r_{80} , r_{31} , and r_{82} . The distance of adjacent nodes is 2.4 km. The map shows 2,000 EVs over 24 hours, with colors indicating EV density. An overlaid modified IEEE-9-bus system connects EV loads to PQ buses based on color-coded areas, powered by a wind generator at bus 2 [50]. The specifications of vehicles are from [51], their proportion is decided by the market share. The unit price of Li-ion battery and ultracapacitor is 128 \$\/kWh and 2500 \$\/kWh respectively [52]. The lifecycle of the battery ends with 20% capacity loss [40]. It is assumed that the capacity of the extra device is 10% of main battery. (Dis)charging rates and efficiency of battery are 6 kW and 95%, and ultracapacitor fully (dis)charges within the time interval. MATPOWER is used for power flow calculation [53]. The constraint's settings are $wt_{max}=1$ h, $th^{EV}=70\%$, $v_{max}=1.05$, v_{min} =0.95, n_{max} =50, soc_{max} =1, and soc_{min} =0. The penalty weights w_1^p and w_2^p are assigned with sufficiently large values to treating them as hard constraints, i.e., -999. Renewable energy available for free during surplus periods i.e., 10:00-16:00 and 20:00-22:00. The initial SoC distributions of the battery and ultracapacitor in each scenarios are generated by Monte Carlo method.

B. Deployment Results

Deployment results are listed in Table 7. The planned BCS is scattered throughout the road network. In the RES area, more BCS and servers are planned, such as node 6 and 111. In S2-S6, the cost of infrastructures are enhanced since the involvement of trading. In cases where main battery includes trading, charging demand is higher. Notably, S4 incurs minimal extra costs among trading scenarios. There are 6 methods are selected for comparison, which are widely applied in EV-related case, including: GA, HC, PSO, and simulated annualing (SA) [54-56]. Also, ablation experiments are conducted, and the comparison algorithms include GAHC and GAPSO. The difference between the two algorithms and our method lies in the removal of corresponding components, and other parameters are the same. Table 8 presents the relevant comparative analysis, emphasizing cost^{driver} costoperator, and score, as key parameters linked to the objective. Bold text identifies the best-performing result. S4 yielding the highest scores due to the lower driver cost with trading and less extra construction cost. Results of waiting time, accessibility evaluation, and training process are shown in Fig. 12. Limitations for wt^{max} and propass are depicted in green and red areas. wt^{max} is within the green part, and pro^{pass} exceeds the red region. Fig. 12 (c) illustrates the training cycle in relation to peak score. It is clearly indicated that our proposed algorithm demonstrates superior performance relative to benchmark algorithms.

As discussed in the introduction, M/M/s is the most widely used model for estimating waiting time, with the input of a constant EV load (arrival rate). While in our work M(t)/M(t)/s is utilized, time-varying load can be considered. Two models' impacts on deployment tasks are compared in S1. D1 and D2

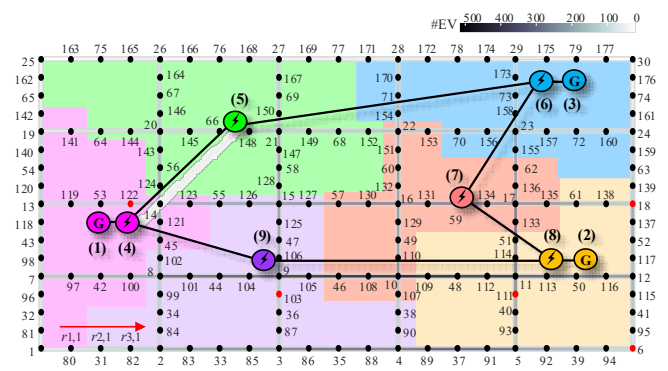


Fig. 11. Road network with IEEE 9 bus overlaid.

TABLE VII

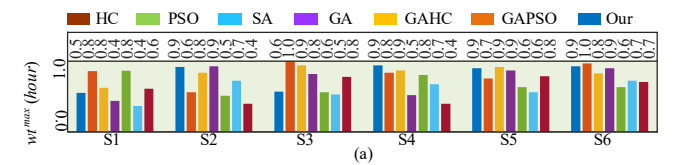
RESULTS OF OPTIMAL DEPLOYMENT OF 6 SCENARIOS

	BCS locations	# servers	cost operatorr
S1	6, 18, 103, 111, 122	14, 3, 5, 31, 2	1.5×10 ⁵ \$
S2	6, 18, 103, 111, 122	35, 13, 10, 32, 14	2.0×10^{5} \$
S3	6, 18, 103, 111, 122	13, 6, 2, 50, 8	1.7×10^{5} \$
S4	6, 18, 103, 111, 122	16, 4, 3, 32, 4	1.5×10^{5} \$
S5	6, 10, 18, 103, 111, 122	19, 50, 3, 11, 32, 17	2.5×10^{5} \$
S6	6, 18, 103, 111, 122	33, 12, 17, 40, 34	2.3×10 ⁵ \$

TABLE VIII

COMPARISONS OF OPTIMIZATION ALGORITHMS

		HC	PSO	SA	GA	GAHC	GAPSO	Our
	S1	1.5	1.6	1.6	1.5	1.5	1.5	1.5
\$ (s	S2	1.3	1.3	1.3	1.4	1.3	1.4	1.3
driv)-1	S3	1.3	1.2	1.2	1.3	1.3	1.3	1.3
cost driver (×10 ⁻¹ \$)	S4	1.0	1.1	1.1	1.0	1.0	1.1	1.0
8 0	S5	1.3	1.2	1.2	1.3	1.3	1.3	1.3
	S6	0.9	1.0	0.9	0.9	0.9	0.9	0.9
	S1	2.7	1.9	2.4	1.5	1.9	1.8	1.5
stor	S2	3.8	3.2	3.7	2.8	2.3	2.4	2.0
cost ^{op erator} $(\times 10^5\$)$	S3	3.5	3.7	3.8	2.8	2.6	2.4	1.7
ost ^{opera} (×10 ⁵ !	S4	3.0	2.6	2.5	2.6	2.0	1.9	1.5
8 ~	S5	3.8	3.2	3.7	2.8	2.6	2.5	2.5
	S6	3.6	3.6	3.5	3.3	2.3	3.6	2.3
	S1	3.1	4.0	3.3	3.2	4.1	4.3	5.0
	S2	2.5	2.8	2.5	3.0	3.6	3.4	4.0
0^{-1}	S3	2.6	2.8	2.5	3.1	3.3	3.4	4.5
score (×10-1	S4	3.2	3.4	3.5	3.5	4.3	4.3	5.4
_	S5	2.4	2.4	2.3	2.6	3.3	3.4	3.4
	S6	2.9	2.8	3.0	3.1	4.0	3.6	4.0



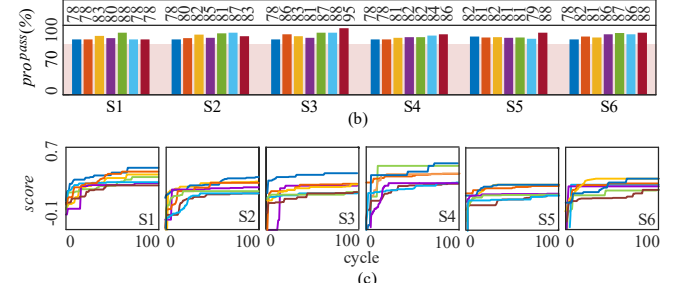


Fig. 12. Comparison of different optimization algorithms. (a) maximum waiting time. (b) accessibility evaluation. (c) training process.

represent deployment schemes based on M(t)/M(t)/s and M/M/s. Both approaches select the same BCSs, yet D2 requires fewer servers than D1, resulting in reduced construction costs. Waiting time is displayed in two rows: the

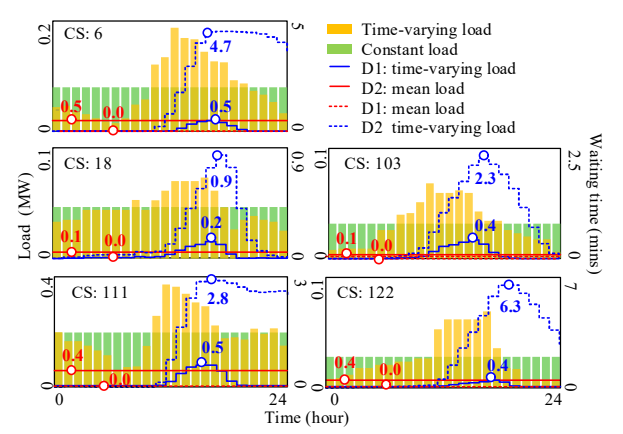


Fig. 13. Waiting time estimation of D1 and D2 by M(t)/M(t)/s or M/M/s.

TABLE IX COMPARISON OF RESULTS OF D1 AND D2

		D1: $M(t)/M(t)/s$	D2: M/M/s
BCS locations		6, 18, 103, 111, 122	6, 18, 103, 111, 122
	# servers	14, 3, 5, 31, 2	8, 3, 4, 14, 2
$cost^{operatorr}$ (10 ⁶ \$)		atorr (10 ⁶ \$) 0.15	
max (1.)	Cooresponding model	0.5	0.5
$vt^{max}(h)$	Crosscheck	0.0	6.3

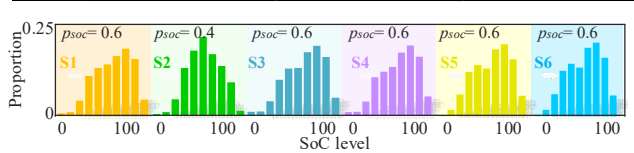


Fig. 14. SoC level of 6 scenarios at the end of the day, where p_{soc} is the proportion of SoC>0.7.

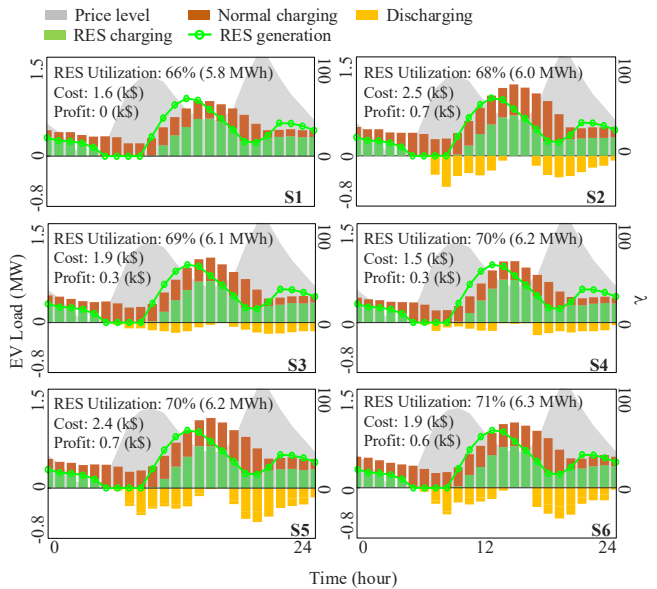


Fig. 15. EV (dis)charging load of 6 scenarios with indicators of RES utilization, cost and profit.

first row presents waiting times derived directly from each model (D1 using M(t)/M(t)/s and D2 using M/M/s), with both yielding a waiting time of 0.5, within acceptable limits. The second row shows a cross-checked waiting time, with D2 assessed under M(t)/M(t)/s, resulting in a maximum value of 6.3 h, which significantly exceeds the constraint. This discrepancy demonstrates that M/M/s may underestimate waiting times, risking a QoS lower than anticipated. Thus,

TABLE X

INDICATORS UNDER DIFFERENT BEHAVIOR-RELATED PARAMETERS								
			S1	S2	S3	S4	S5	S6
$cost^{dm\sigma^*}(imes 10^{-1}\$)$		0.1	1.4	1.3	1.3	1.1	1.2	0.8
	k	0.5	1.4	1.2	1.2	1.1	1.2	0.8
		1.0	1.3	1.2	1.2 1.4	1.1	1.2 1.2	0.8
	Δχ	0	1.6	1.6	1.4	1.1	1.2	0.9
		5	1.3	1.2	1.2	1.0	1.2	0.8
		10	1.2	1.2	1.2	0.9	1.1	0.8
	X_p^{ch}	30	1.2	1.3	1.2	1.1	1.0	0.8
		60	1.3	1.3	1.3	1.1	1.1	0.8
		90	1.5	1.3	1.4	1.1	1.2	0.9
		10	1.2	1.1	1.1	0.9	1.0	0.8
	X_q^{ch}	40	1.3	1.2	1.2	1.1	1.2	0.8
		70	1.3	1.3	1.3	1.1	1.3	0.8
		30	-	1.2	1.3	1.0	1.2	0.8
	X_p^{dch}	60	-	1.3	1.3	1.1	1.2	0.8
		90	-	1.3 1.3	1.3 1.3	1.2	1.2	0.8
		10	-	1.2	1.3	1.0	1.1	0.8
	χ_q^{dch}	40	-	1.2	1.3 1.3	1.1	1.2	0.8
		70	-	1.3	1.3	1.1	1.3	0.8
		0.1	4.6	5.7	5.0	6.0	4.9	7.4
	k	0.5	4.6	6.4	4.8	5.6	4.9	6.8
		1.0	4.7	6.4	4.8	5.6	4.9	6.8
		0	3.1	3.5	4.3	5.5	4.6	6.5
	Δx	5	5.1	6.5	5.4	6.1	5.1	6.8
		10	5.1	6.2	4.7	5.8	5.1	6.4
Д.		30	5.1	5.3	5.4	5.9	5.4	7.4
€	\mathcal{X}_p^{ch}	60	4.8	6.1	4.9	5.6	5.1	6.9
energ ^{srer} (MWh)		90	4.2	7.2	4.6	5.4	5.0	6.8
2500	-4	10	5.5	6.4	5.7	6.9	6.4	8.5
ner	\mathcal{X}_q^{ch}	40	4.6	5.9	4.7	5.4	4.9	6.8
Ö		70	4.6	4.6	4.6	5.3	4.6	6.7
	deh	30	-	7.1	5.2	6.4	5.2	6.9
	X_p^{dch}	60	-	5.4	4.6	5.6	5.1	6.8
		90	-	4.9	4.7	5.3	4.8	6.8
	dch	10	-	6.2	5.0	6.1	6.0	7.0
	X_q^{dch}	40	-	5.8	4.8	5.5	4.9	6.8
		70	- 10.5	5.8	4.8	5.3	4.5	6.8
	,	0.1	12.5	11.8	11.8	11.8	11.8	11.7
	k	0.5	12.5	11.8	11.7	11.8	11.8	11.8
		1.0	12.5	11.8	11.7 12.2	11.9	11.8	11.8
		0	12.5	11.8	12.2	12.2	11.9	11.8
	Δx	5	12.5	11.7	11.9	11.8	11.8	11.8
S		10 30	12.2 12.4	11.7 11.8	11.8 11.8	11.9 11.8	11.8	11.8
loss ^{trans} (×10 ⁻¹ MW)	_ch	60		11.8		11.8		11.7
	X_p^{ch}	90	12.5 12.5	11.7	11.8 11.8	11.8 11.8	11.8 11.8	11.7 11.7
×				11.7	11.8		11.0	
) su	χ_q^{ch}	10	12.3	11.7		11.9	11.8	11.8
st.Stra		40	12.3	11.8	11.9	11.9	11.9	11.8
los		70	12.3	11.8 11.8	11.9	11.9	11.9	11.9
	X_p^{dch}	30 60	-	11.8	11.8	11.8	11.9	11.8
	X_p		-	11.8	12.0	12.0	11.9	11.8
		90	-	11.8	12.0	12.0	12.0	11.8
	X_q^{dch}	10 40	-		11.8	11.9	11.9	11.8
		40 70	-	11.8 11.9	11.9	11.9	11.9	11.8
		/0		11.9	11.8	11.9	11.9	11.8

adopting the M(t)/M(t)/s model is essential for a realistic estimation and improved deployment outcomes.

C. Drivers' Performances

Based on deployment result, drivers' behavior is further studied with the results from 2000 drivers over 30 days. SoC is an essential metric, Fig. 14 illustrates the SoC distribution at the end of trips, using SoC > 70% as a threshold. It is noted that psoc is lowest in S2, where only the main battery is used for both travel and trading, thus potentially increasing range anxiety. EV loads are depicted in Fig.15 with electricity prices in the background shaded gray and load represented by bars: red for regular charging, green for renewable charging, and yellow for discharging. The renewable energy generation curve is overlaid as green line. The top left corner of the figure displays three metrics: average daily renewable utilization, total cost, and total profit. Across the 6 scenarios, charge-

		SI	S2	83	S4	85	S6
	2	1.5	1.1	1.2	1.0	1.2	0.7
P1	5	1.5	0.5	0.9	0.7	0.6	0.1
	10	1.5	-0.5	0.4	0.2	-0.4	-0.9
	0.5	1.1	1.0	1.0	0.8	1.1	0.7
P2	0.2	1.0	0.9	0.9	0.7	0.9	0.6
	0.1	0.9	0.8	0.9	0.6	0.9	0.5
	0.5	1.0	0.8	0.8	0.7	0.8	0.5
P3	0.1	0.7	0.4	0.5	0.4	0.4	0.3
	0.0	0.6	0.4	0.4	0.4	0.3	0.2
	0.3	1.2	1.0	1.0	0.8	1.0	0.7
P4	0.5	1.0	0.9	0.9	0.7	0.9	0.6
	1.0	0.6	0.4	0.4	0.3	0.3	0.2

discharge patterns are similar, with load generally rising around 9:00, peaking between 12:00 and 13:00. Discharging tends to concentrate during high-price periods. Comparing across the six scenarios, the integration of trading leads to a marked increase in charging load. Significant discharging is observed in S2, S5, and S6, as these scenarios allow the main battery to participate in trading. Additionally, the renewable energy utilization rate increases across trading-enabled scenarios S2–S6. Scenarios S4 and S6, in particular, show potential for driver profit due to the absence of degradation costs from supercapacitor. These results affirm the benefits of renewable energy integration in EVEN scenarios and the advantages of ultracapacitor participation in trading.

Next, we perform sensitivity analysis on key parameters, using indicators: cost^{driver}, e^{res}, and loss^{trans}, representing unit driver cost, daily average renewable energy consumption, and grid transmission loss, respectively. Calculations of cost^{driver} has been given in (23)-(26). Performances under different behavioral parameters are compared in Table 10. It provides guideline to reduce cost for drivers. Drivers should lower k, x_q^{ch} , x_p^{ch} , x_q^{dch} , and x_p^{dch} , while increase Δx to lower $cost^{driver}$. This means improving decision-making execution ability, reducing driving anxiety, and moderately increasing price sensitivity. In scenarios with a second device, slightly broadening the price range is advantageous. Comparing S1 with other scenarios, trading can reduce the cost of driver. Higher energy^{res} are associated with lower cost^{driver}. Ultracapacitor has higher consumption compared to battery, and two trading devices result in higher energy^{res}, i.e., S5>S3 and S6>S4. Additionally, trading positively impacts loss^{trans}, reducing grid losses. Among these indicators, S6 outperforms other trading scenarios since it achieves lowest driver cost, transmission loss, and highest RES utilization, but the cost for buying the ultracapacitor is not accounted, which is expensive to afford.

Impacts of different policies on $cost^{driver}$ are studied, including: (P1) higher selling prices, (P2) lower buying prices, (P3) reduced k_w (a key degradation parameter in Eq. (18)), and (P4) proportional subsidies for degradation. Results are shown in Table 11. Among these measures, increasing the selling price provides the highest profit for drivers, even covering travel costs in S2, S5, and S6. Lowering the buying price has a limited effect, as drivers already benefit from free renewable energy. Reducing degradation costs also improves profitability, but $cost^{driver}>0$. Therefore, the effectiveness of providing higher selling prices are highlighted for improving driver profitability.

VI. CONCLUSION

In this paper, a stochastic driver's behavior model and a BCS deployment optimization approach are developed for EVEN for 6 trading scenarios: (S1) no trade; (S2) trade in main battery; (S3) trade in extra battery; (S4) trade in extra ultracapacitor; (S5) trade in both main and extra battery; (S6) trade in both main battery and ultracapacitor. The proposed stochastic (dis)charging behavior model is based on Markov method, considering personal characteristic, SoC, real-time electricity price. It is able to estimate load pattern in both microscopic and macroscopic levels, examining the impact of different behaviors on individual and overall load. BCS deployment is designed by minimizing both drivers and operators' cost, with the constraints of QoS and grid voltage stability, and solved by the proposed hybrid optimization algorithm.

In experiments of driver's behavior model by two real-world datasets, the model effectively fits charging patterns with MAPE, MSE, and RMSE. The parameter selection algorithm achieves an efficiency improvement of 89.1% comparing with grid search approach with dimension of $\varepsilon(t)=3$. Among S1-S6, trading increases charging demand, and ultracapacitors lead to earlier and higher peaks compared to batteries. Sensitivity analysis reveals that range anxiety increases charging while reducing discharging load. Price-sensitive drivers tend to focus on trading during peak and off-peak price periods. The model offers profitability suggestions for drivers, such as improving decisiveness, reducing range anxiety, and maintaining relatively higher price sensitivity.

For the experiment of BCS deployment, the effectiveness of the proposed algorithm is demonstrated by ablation comparisons. Comparing S1 to S6, trading necessitates additional chargers, raising construction costs, and more BCSs are constructed in RES areas. For maximum waiting time calculation, M/M/s underestimate maximum waiting times compared with M(t)/M(t)/s, degrading QoS. The benefits of EVEN is verified as energy trading lowers daily costs, enhances renewable energy utilization, and reduces grid transmission losses, with S6 performing best in these areas. The benefits of ultracapacitor in energy trading is also verified. For drivers, it helps eliminate degradation cost hence improve their cost. For BCS operator, the exclusive use of ultracapacitors leads to lower additional cost, as it enables quick trading and reducing charger demand. To further attract drivers in EVEN, providing higher selling prices is highlighted as effective financial strategies compared with other policies, such as lower buying prices and reduce degradation cost.

However, our work overlooks real-world complexities such as EV energy efficiency variability, diverse usage patterns, and real-time traffic conditions. Addressing these aspects in future work will enhance the robustness and practicality of demand modeling and deployment.

APPENDIX

The settings for the comparison algorithms in part B, section VI is presented as below.

TABLE XII SETTINGS OF THE COMPARISON ALGORITHMS

Algorithm	Settings				
HC	Stochastic hill climbing is used.				
	 With the initial population of 50, the solutions are formed randomly. 				
	Top 5 solutions are selected to generate neighbours with the number of 10.				
	The local change to current solution is formed randomly.				
	4. The algorithm stops when reach the number of iterations of 100.				
GA	 With the initial population of 50, the candidate solutions are formed randomly. 				
	Rank-based selection is used to choose parents, and the crossover rate is selected as 0.9.				
	3. Crossover with uniform method.				
	4. The probability of mutation is set as 0.2 to change the genes randomly.				
	5. The algorithm stops when reach the number of iterations of 100.				
SA	 Initial temperature as 1000; ending temperature as 0.1, alpha=0.98. literation in each temperature = 50. 				
	Geometric cooling is applied to decide the cooling schedule.				
	Cooling rate is set as 0.98, so as to allow more thorough exploration of search space.				
	4. Neighbour generation, which can refer HC method.				
	5. The algorithm stops when reach the number of iterations of 100.				
PSO	 Initial swarm size as 50. Randomly initialize the position and velocity of each particle in the swarm. 				
	2. Set parameters: inertia weight =0.9; cognitive coefficient = 1.5; social coefficient = 1.5; velocity limits for x: ±1, for n is ± maximum number of servers=50.				
	3. Based on given parameters to update velocity and position.				
	4. Update particles and repeat until reach the number of iterations of 100.				
GAPSO	Parameters are the same with GA and PSO.				
GAHC	Parameters are the same with GA and HC.				
Our	Parameters are the same with GA, PSO, and HC.				

REFERENCES

- A. T. Al-Awami and E. Sortomme, "Coordinating vehicle-to-grid services with energy trading," *IEEE Transactions on Smart Grid*, vol. 3, no. 1, pp. 453-462, Nov. 2012.
- [2] K. T. Chau, Energy systems for electric and hybrid vehicles. The Institution of Engineering and Technology, 2016.
- [3] K. T. Chau, Pure electric vehicles. in alternative fuels and advanced vehicle technologies for improved environmental performance – towards zero carbon transportation. (Ed.) R. Folkson. Woodhead Publishing, 2014, pp. 655-684
- [4] A. Y. S. Lam, K. C. Leung, and V. O. K. Li, "Vehicular energy network," IEEE Transactions on Transportation Electrification, vol. 3, no. 2, pp. 392-404, Jan. 2017.
- [5] P. Yi, T. Zhu, B. Jiang, B. Wang, and D. Towsley, "An energy transmission and distribution network using electric vehicles," in 2012 IEEE International Conference on Communications (ICC), 2012, pp. 3335-3339.
- [6] C. C. T. Chow, A. Y. S. Lam, W. Liu, and K. T. Chau, "Multisource-multidestination optimal energy routing in static and time-varying vehicular energy network," *IEEE Internet of Things Journal*, vol. 9, no. 24, pp. 25487-25505, Aug. 2022.
- [7] S. S. Fazeli, S. Venkatachalam, R. B. Chinnam, and A. Murat, "Two-stage stochastic choice modeling approach for electric vehicle charging station network design in urban communities," *IEEE Transactions on Intelligent Transportation Systems*, vol. 22, no. 5, pp. 3038-3053, Mar. 2021.
- [8] Canada tests its first V2G for medium and heavy-duty EVs. Accessed: Mar. 2024. [Online]. Available: https://shorturl.at/fko12
- [9] S. S. Shinde and D. Tarchi, "A markov decision process solution for energy-saving network selection and computation offloading in vehicular networks," *IEEE Transactions on Vehicular Technology*, vol. 72, no. 9, pp. 12031-12046, Apr. 2023.
- [10] J. Qi, C. Lai, B. Xu, Y. Sun, and K. S. Leung, "Collaborative energy management optimization toward a green energy local area network," *IEEE Transactions on Industrial Informatics*, vol. 14, no. 12, pp. 5410-5418, Jan. 2018.
- [11] T. Fu, C. Wang, and N. Cheng, "Deep-learning-based joint optimization of renewable energy storage and routing in vehicular energy network," *IEEE Internet of Things Journal*, vol. 7, no. 7, pp. 6229-6241, Jan. 2020.
- [12] S. Liu, L. Wang, J. Hu, and Z. Zhou, "A stochastic charging station deployment model for electrified taxi fleets in coupled urban transportation and power distribution networks," *IEEE Transactions on Sustainable Energy*, vol. 15, no. 2, pp. 1138-1150, Nov. 2024.
- [13] F. Ahmad, A. Iqbal, I. Asharf, M. Marzband, and I. Khan, "Placement and capacity of ev charging stations by considering uncertainties with energy management strategies," *IEEE Transactions on Industry Applications*, pp. 1-10, Mar. 2023.
- [14] Y. Zhou, X. C. Liu, R. Wei, and A. Golub, "Bi-objective optimization for battery electric bus deployment considering cost and environmental equity," *IEEE Transactions on Intelligent Transportation Systems*, vol. 22, no. 4, pp. 2487-2497, Dec. 2021.

- [15] Z. Zhao, C. K. M. Lee, J. Ren, and Y. P. Tsang, "Optimal ev fast charging station deployment based on a reinforcement learning framework," *IEEE Transactions on Intelligent Transportation Systems*, vol. 24, no. 8, pp. 8053-8065, Apr. 2023.
- [16] Y. Zhang, Y. Wang, F. Li, B. Wu, Y. Y. Chiang, and X. Zhang, "Efficient deployment of electric vehicle charging infrastructure: simultaneous optimization of charging station placement and charging pile assignment," *IEEE Transactions on Intelligent Transportation Systems*, vol. 22, no. 10, pp. 6654-6659, May. 2021.
- [17] F. Ahmad, A. Iqbal, I. Ashraf, M. Marzband, and I. Khan, "Optimal location of electric vehicle rapid charging stations in power distribution network and transportation network with V2G strategies," in 2021 IEEE Transportation Electrification Conference (ITEC-India), 2021, pp. 1-5.
- [18] R. Chakraborty, D. Das, and P. Das, "Optimal placement of electric vehicle charging station with v2g provision using symbiotic organisms search algorithm," in 2022 IEEE International Students' Conference on Electrical, Electronics and Computer Science (SCEECS), 2022, pp. 1-6.
- [19] G. Wu et al., "Multi-objective optimization of integrated energy systems considering renewable energy uncertainty and electric vehicles," *IEEE Transactions on Smart Grid*, pp. 1-1, Mar. 2023.
- [20] Y. Sui, P. Yi, X. Liu, and T. Zhu, "Energy transport station deployment in electric vehicles energy internet," *IEEE Access*, vol. 7, pp. 97986-97995, Jul. 2019.
- [21] J. Antoun, M. E. Kabir, R. F. Atallah, and C. Assi, "A data driven performance analysis approach for enhancing the QoS of public charging stations," *IEEE Transactions on Intelligent Transportation Systems*, vol. 23, no. 8, pp. 11116-11125, Aug. 2022.
- [22] X. Gan, H. Zhang, G. Hang, Z. Qin, and H. Jin, "Fast-charging station deployment considering elastic demand," *IEEE Transactions on Transportation Electrification*, vol. 6, no. 1, pp. 158-169, Jan. 2020.
- [23] Q. Yang, S. Sun, S. Deng, Q. Zhao, and M. Zhou, "Optimal sizing of pev fast charging stations with markovian demand characterization," *IEEE Transactions on Smart Grid*, vol. 10, no. 4, pp. 4457-4466, Jul. 2019.
- [24] M. H. Bahmani, M. Esmaeili Shayan, and D. Fioriti, "Assessing electric vehicles behavior in power networks: A non-stationary discrete Markov chain approach," *Electric Power Systems Research*, vol. 229, p. 110106, Jan. 2024.
- [25] G. Gruosso, A. Mion, and G. Storti Gajani, "Forecasting of electrical vehicle impact on infrastructure: Markov chains model of charging stations occupation," eTransportation, vol. 6, pp. 100083, Oct. 2020.
- [26] Z. Fotouhi, M. R. Hashemi, H. Narimani, and I. S. Bayram, "A general model for ev drivers' charging behavior," *IEEE Transactions on Vehicular Technology*, vol. 68, no. 8, pp. 7368-7382, Jun. 2019.
- [27] M. Yilmaz and P. T. Krein, "Review of the impact of vehicle-to-grid technologies on distribution systems and utility interfaces," *IEEE Transactions on Power Electronics*, vol. 28, no. 12, pp. 5673-5689, Nov. 2013
- [28] W. Liu, K. T. Chau, C. C. T. Chow, and C. H. T. Lee, "Wireless energy trading in traffic internet," *IEEE Transactions on Power Electronics*, vol. 37, no. 4, pp. 4831-4841, Oct. 2022.

- [29] K. W. Hu, P. H. Yi, and C. M. Liaw, "An EV SRM drive powered by battery/supercapacitor with G2V and V2H/V2G capabilities," *IEEE Transactions on Industrial Electronics*, vol. 62, no. 8, pp. 4714-4727, Jan. 2015
- [30] Vehicle-to-Grid (V2G) Market—Global Size, Share & Industry Analysis. Accessed: Mar. 2024. [Online]. Available: https://shorturl.at/ehjEJ
- [31] P. Yi, T. Zhu, B. Jiang, R. Jin, and B. Wang, "Deploying energy routers in an energy internet based on electric vehicles," *IEEE Transactions on Vehicular Technology*, vol. 65, no. 6, pp. 4714-4725, Mar. 2016.
- [32] Y. Wang, Z. Su, Q. Xu, T. Yang, and N. Zhang, "A novel charging scheme for electric vehicles with smart communities in vehicular networks," *IEEE Transactions on Vehicular Technology*, vol. 68, no. 9, pp. 8487-8501, Jun. 2019.
- [33] P. Liu et al., "Joint route selection and charging discharging scheduling of EVs in V2G energy network," *IEEE Transactions on Vehicular Technology*, vol. 69, no. 10, pp. 10630-10641, Aug. 2020.
- [34] X. Zhang, Y. Xu, S. Lu, C. Lu, and Y. Guo, "Joint planning of distributed PV stations and EV charging stations in the distribution systems based on chance-constrained programming," *IEEE Access*, vol. 9, pp. 6756-6768, Jan. 2021.
- [35] T. Y. Zhang, Y. Yang, Y. T. Zhu, E. J. Yao, and K. Q. Wu, "Deploying public charging stations for battery electric vehicles on the expressway network based on dynamic charging demand," *IEEE Transactions on Transportation Electrification*, vol. 8, no. 2, pp. 2531-2548, Jan. 2022.
- [36] S. M. Kandil, A. Abdelfatah, and M. A. Azzouz, "Optimization approaches for fast charging stations allocation and sizing: a review," *IEEE Access*, vol. 12, pp. 46741-46763, Mar. 2024.
- [37] J. H. D. a. A. Rustichini, "State-dependent utility and decision theory," Handbook of Utility Theory, vol. 2, pp. 839–892, 2004.
- [38] J. Tan and L. Wang, "Real-time charging navigation of electric vehicles to fast charging stations: a hierarchical game approach," *IEEE Transactions on Smart Grid*, vol. 8, no. 2, pp. 846-856, Aug. 2017.
 [39] T. Zhang, X. Chen, Z. Yu, X. Zhu, and D. Shi, "A monte carlo simulation
- [39] T. Zhang, X. Chen, Z. Yu, X. Zhu, and D. Shi, "A monte carlo simulation approach to evaluate service capacities of ev charging and battery swapping stations," *IEEE Transactions on Industrial Informatics*, vol. 14, no. 9, pp. 3914-3923, 2018.
- [40] H. Farzin, M. Fotuhi-Firuzabad, and M. Moeini-Aghtaie, "A practical scheme to involve degradation cost of lithium-ion batteries in vehicle-to-grid applications," *IEEE Transactions on Sustainable Energy*, vol. 7, no. 4, pp. 1730-1738, Jul. 2016.
 [41] P. K. Linda Green, Anthony Svoronos, "Some effects of nonstationarity on
- [41] P. K. Linda Green, Anthony Svoronos, "Some effects of nonstationarity on multiserver markovian queueing systems," *Operations Research*, vol. 39, no. 3, pp. 502-511, Jun. 1991.
- [42] S. Molaei, H. Moazen, S. Najjar-Ghabel, and L. Farzinvash, "Particle swarm optimization with an enhanced learning strategy and crossover operator," *Knowledge-Based Systems*, vol. 215, p. 106768, Jan. 2021.
- [43] Electric vehicle charging sessions dundee. Accessed: Mar. 2024. [Online]. Available: https://data.dundeecity.gov.uk/dataset/ev-charging-data
- [44] Charging profiles: regular charging. Accessed: Mar. 2024. [Online]. Available: https://platform.elaad.io/analyse/charging/
- [45] Average electric car kWh per mile. Accessed: Mar. 2024. [Online]. Available: https://ecocostsavings.com/average-electric-car-kwh-per-mile/
- [46] M. Shafie-khah et al., "Optimal behavior of electric vehicle parking lots as demand response aggregation agents," *IEEE Transactions on Smart Grid*, vol. 7, no. 6, pp. 2654-2665, Nov. 2016.
- [47] Eupore's leading power market: day ahead prices. Accessed: Mar. 2024.
 [Online]. Available: https://www.nordpoolgroup.com/en/Market-data1/#/n2ex/table
- [48] P. Diaz-Cachinero, J. I. Muñoz-Hernandez, and J. Contreras, "A microgrid model with ev demand uncertainty and detailed operation of storage systems," *IEEE Transactions on Industry Applications*, vol. 58, no. 2, pp. 2497-2511, Dec. 2022.
- [49] J. Zhou, L. Zhang, and G. Zhang, "Two-level optimization model of integrated energy system based on dynamic pricing mechanism," *IEEE Transactions on Industry Applications*, vol. 60, no. 1, pp. 1048-1057, Sept. 2024.
- [50] Wind Power Generation Data. Accessed: Mar. 2024. [Online]. Available: https://www.kaggle.com/datasets/jorgesandoval/wind-power-generation?resource=download&select=TransnetBW.csv
- [51] H. Liang, Z. Lee, and G. Li, "A calculation model of charge and discharge capacity of electric vehicle cluster based on trip chain," *IEEE Access*, vol. 8, pp. 142026-142042, Aug. 2020.
- [52] P. K. S. Roy, H. B. Karayaka, J. He, and Y. H. Yu, "Economic comparison between battery and supercapacitor for hourly dispatching wave energy converter power," in 2020 52nd North American Power Symposium (NAPS), 2021, pp. 1-6.
- [53] R. D. Zimmerman, C. E. Murillo-Sánchez, and R. J. Thomas, "MATPOWER: steady-state operations, planning, and analysis tools for power systems research and education," *IEEE Transactions on Power Systems*, vol. 26, no. 1, pp. 12-19, Jun. 2011.

- [54] Y. Liu, Z. Liu, J. Shi, G. Wu, and W. Pedrycz, "Two-echelon routing problem for parcel delivery by cooperated truck and drone," *IEEE Transactions on Systems, Man, and Cybernetics: Systems*, vol. 51, no. 12, pp. 7450-7465, Feb. 2021.
- [55] H. Ma, L. Chu, J. Guo, J. Wang, and C. Guo, "Cooperative adaptive cruise control strategy optimization for electric vehicles based on SA-PSO with model predictive control," *IEEE Access*, vol. 8, pp. 225745-225756, Dec. 2020
- [56] X. Gao, K. W. Chan, S. Xia, X. Zhang, K. Zhang, and J. Zhou, "A multiagent competitive bidding strategy in a pool-based electricity market with price-maker participants of WPPs and EV aggregators," *IEEE Transactions on Industrial Informatics*, vol. 17, no. 11, pp. 7256-7268, Feb. 2021



Yao Tang (Student Member, IEEE) received the B.Eng. degree from Beijing Forestry University, China in 2019, and received the M.Eng. degree from Hunan University, China in 2021. She is currently working toward the Ph.D. degree in electrical and electronic engineering at the Department of Electrical and Electronic Engineering, the University of Hong Kong. Her current research interests include electric vehicle, optimization theory and artificial intelligence for industrial applications.



Wei Liu (Senior Member, IEEE) received the B.Eng. and M.Eng. degrees in electrical engineering from China University of Petroleum, Qingdao, China, and a Ph.D. degree in electrical and electronic engineering from The University of Hong Kong (HKU), Hong Kong, China, in 2014, 2017, and 2021, respectively.

He is currently an Assistant Professor at the Research Centre for Electric Vehicles and the Department of Electrical and Electronic Engineering

at the Hong Kong Polytechnic University (PolyU). Dr. Liu served as a Postdoctoral Fellow and a Research Assistant Professor from 2021 to 2023, and he is now an Honorary Assistant Professor at the Department of Electrical and Electronic Engineering, HKU. He also worked as a Visiting Researcher with Nanyang Technological University, Singapore (NTU), in 2019. His research interests include wireless power transfer, power electronics, biomedical power electronics, and electric vehicle technologies.

Dr. Liu was the recipient of the Power Engineering Prize from HKU, the Excellent Paper Award, and the Best Presentation Award from international conferences in the area of Electric Vehicles and Transportation Electrification. He is also a Guest Associate Editor of *IEEE Journal of Emerging and Selected Topics in Power Electronics (JESTPE)*, Guest Editor of international journals, and Session Chair of international conferences.



K. T. Chau (Fellow, IEEE) received the B.Sc. (Eng.), M.Phil., and Ph.D. degrees in electrical and electronic engineering from The University of Hong Kong, Hong Kong, in 1988, 1991, and 1993, respectively. Currently, he serves as Chair Professor of Electrical Energy Engineering at the Research Centre for Electric Vehicles and Department of Electrical and Electronic Engineering, The Hong Kong Polytechnic University. His research interests include electric and hybrid vehicles, power

electronics and drives, and renewable energies. He is the author of nine books and more than 350 journal papers.

Prof. Chau is a Fellow of the Institution of Engineering and Technology (IET), U.K., and of the Hong Kong Institution of Engineers. He is also a Coeditor of the Journal of Asian Electric Vehicles. He is a Chartered Engineer. He was the recipient of the Changjiang Chair Professorship from the Ministry of Education, China, and the Environmental Excellence in Transportation Award for Education, Training, and Public Awareness from the Society of Automotive Engineers International.



Yunhe Hou (Senior Member, IEEE) received the B.E. and Ph.D. degrees in electrical engineering from the Huazhong University of Science and Technology, Wuhan, China, in 1999 and 2005, respectively. He was a Postdoctoral Research Fellow with Tsinghua University, Beijing, China, from 2005 to 2007, and a Postdoctoral Researcher with Iowa State University, Ames, IA, USA, and the University College Dublin, Dublin, Ireland, from 2008 to 2009. He was also a Visiting Scientist with the Laboratory for Information

and Decision Systems, Massachusetts Institute of Technology, Cambridge, MA, USA, in 2010. He has been a Guest Professor with the Huazhong University of Science and Technology, China, since 2017, and an Academic Adviser of China Electric Power Research Institute since 2019. He joined as a Faculty with the University of Hong Kong, Hong Kong, in 2009, where he is an Associate Professor in the Department of Electrical and Electronic Engineering. He was an Associate Editor of IEEE TRANSACTIONS ON SMART GRID from 2016 to 2021. He is currently an Associate Editor of IEEE TRANSACTIONS POWER SYSTEMS and the Journal of Modern Power Systems and Clean Energy.



Jian Guo (Member, IEEE) was born in Hubei, China, in 1995. He received a B.S. degree in electronic information engineering from China University of Mining and Technology, Xuzhou, China, in 2017, and a Ph.D. degree in electrical engineering from Hunan University, Changsha, China, in 2022. Currently, he is a Postdoctoral Fellow at the Department of Electrical and Electronic Engineering, at the University of Hong Kong. His research interests include power electronic converters,

wireless power transfer, and renewable energies.